Hydrological hotspots of climatic influence in Brazil: A two-step regularization approach

Christopher E. Ndehedehe[a], Gebremedhin G. Haile[b,c], Nathan O. Agutu[d], Vagner G. Ferreira[e], Augusto Getirana[f,g], Onuwa Okwuashi[h]

[a] *Australian Rivers Institute and Griffith School of Environment & Science, Griffith University, Nathan, Queensland 4111, Australia.*
[b] *Key Laboratory of Water Cycle and Related Land Surface Processes, Institute of Geographic Sciences and Natural Resources Research, Chinese Academy of Sciences, Beijing, China*
[c] *University of Chinese Academy of Sciences, Beijing, China*
[d] *Department of Geomatic Engineering and Geospatial Information systems JKUAT, Nairobi, Kenya*
[e] *School of Earth Sciences and Engineering, Hohai University, Nanjing, China*
[f] *Hydrological Sciences Laboratory, NASA Goddard Space Flight Center, Greenbelt, MD, USA*
[g] *Earth System Science Interdisciplinary Center, University of Maryland, College Park, MD, USA*
[h] *Department of Geoinformatics and Surveying, University of Uyo, P.M.B. 1017, Uyo, Nigeria.*

Abstract

Interest in region-specific assessments of droughts and the need to optimise water resources planning and allocation on a local scale via additional investments in water infrastructures is emerging as novel management initiatives to build drought resilience. In this study, a novel two-step regularization procedure that combines statistical rotation with support vector machine regression (SVMR) is employed to assess and identify hydrological regions in Brazil associated with global climate teleconnection patterns (e.g., ENSO, PDO, etc.). To enhance realistic drought impacts assessments, region-specific attributes of drought and the climate modes associated with its variability and characteristics are studied using standardised precipitation index (SPI) and reanalysis data (MERRA). Compared to other regions, results show that drought variability and its occurrence are relatively higher in the extreme north, north-east, and south of Brazil. The predominance of extreme drought events shows that more than 50% of Brazil was affected by the 1998/1999 drought while areas under droughts in recent times fluctuated between 25% in 2012 and 70% in 2015. Results also show significant association of ENSO (e.g., R^2=28%) and PDO (e.g., R^2=18%) with drought indicators in several climatic hot spots. The synthesis of climate modes as predictors of droughts in the SVMR scheme highlights the influence and importance of the Pacific and Atlantic oceans on drought evolutions in Brazil. The MERRA-derived drought indicator extracted this influence better (e.g., $r = 0.72$) than the SPI and appears to be a more suitable drought metric to understand the impacts of global climate on extreme events in the region.

Keywords: Rainfall, SPI, Drought, Support vector machine, ENSO, Brazil

Email address: c.ndehedehe@griffith.edu.au (Christopher E. Ndehedehe)

1. Introduction

On a global scale, the risks emanating from a rise in drought extremes (e.g., Xu et al., 2019, Basu et al., 2017, Yu et al., 2014, Spinoni et al., 2014, van der Molen et al., 2011) and vulnerability to droughts will produce a complex web of impacts that trickles down to physical, economic, environmental, and social aspects of every day life. For instance, limited water availability and supplies caused by prolonged droughts will translate into multiple risks for food security because of constraints on global supply chain of agricultural produce. Although the impacts of extreme droughts and hydrological variability on gross domestic product and regional and global economy are widely reported (e.g., Rippey, 2015, Hall et al., 2014, Brown and Lall, 2006, Benson and Clay, 1994), drought statistics in several regions of the world where the propensity and vulnerability to extreme drought condition is higher are yet to be fully articulated.

However, the impacts of prolonged extreme drought on water availability in Brazil (Fig. 1) is gradually increasing the awareness of its population to the reality of deleterious impacts of climate (e.g., Melati et al., 2019, Ferreira et al., 2018, Erfanian et al., 2017, Getirana, 2016). This awareness comes as result of the unequivocal impacts of droughts on its socio-economic systems. While estimated financial losses due to agricultural drought is 6 billion US dollars, large depletion rates in groundwater in the semi arid regions of Brazil is perceived as a response to prolonged droughts that occurred during the $2010-2017$ period (Melati et al., 2019, Brito et al., 2018). The quantitative assessment of drought events in Brazil undertaken by Brito et al. (2018) confirm a rise in drought frequency and severity during the $2011-2016$ period. Several important studies focused on drought events in Brazil have been documented and summarised by Ferreira et al. (2018), and the stupendous impacts of extreme drought on the availability of freshwater in Brazil have been highlighted in some reports (e.g., Ndehedehe and Ferreira, 2020a, Awange et al., 2016, Getirana, 2016). Some of these studies, for example, noted the impacts of the unprecedented droughts during the $2012-2015$ period on land water storage and surface displacement (e.g., Ferreira et al., 2018, Erfanian et al., 2017, Getirana, 2016) while others identified the influence of climate modes on drought evolutions in the region (e.g., Marengo et al., 2018, Erfanian et al., 2017, Costa et al., 2016). Given that some of these studies were undertaken with no additional information on drought variability and predictability (e.g., Marengo et al., 2017), further drought studies are warranted to reveal the

intrinsic response of droughts in Brazil to indices of oceanic variability and other important processes of inter-annual variability as was the case with land water storage (e.g., Ndehedehe and Ferreira, 2020b).

The aforementioned drought studies nonetheless, lacked localized information on drought statistics and attributes, and the prediction of climate teleconnections associated with drought evolutions. The notion that management of drought risk requires adequate long-term statistics of the attributes of drought events has been advocated as crucial to policy making and public accountability (e.g., Brito et al., 2018, Marengo et al., 2017, Awange et al., 2016). We argue that if drought varies in time and space and is also influenced by multiple physical mechanisms and bio-physical processes, realistic drought impacts assessments that can support policies on crises management requires localization of drought signals on a smaller scale and an investigation of region-specific climatic factors that drives it variability. Superimposing this on a robust drought statistics and characteristics provides a useful framework for an empirical drought assessment that will improve knowledge on drought evolution, risk mitigation and management in drought-prone regions.

Furthermore, the argument that Standardized Precipitation Index (SPI) computed from averaged rainfall data in estimating drought conditions hides the underlying spatial variability of the index (e.g., Ndehedehe et al., 2016, Ali and Lebel, 2009) created the quest for optimised statistical framework to determine its space–time occurrence (e.g., Agutu et al., 2017, Montazerolghaem et al., 2016, Santos et al., 2010). Such framework would be more useful in drought studies, in view of the fact that temporal analysis of drought indicators as shown in some studies (e.g., Haile et al., 2019, Wang et al., 2018, Mao et al., 2017, Awange et al., 2016) are somewhat insufficient to improve knowledge on drought evolutions and the intrinsic response of some regions to the multi-scale interactions of oceanic processes and drivers. Apart from constraint on data and framework, the complexities of drought contributes to limited knowledge on climate change-induced drought events and their characteristics. This complex nature of drought precludes simplistic explanations and diagnosis of drivers and other interacting factors, e.g., politics, technology, culture (e.g., Cook et al., 2018). To handle some of these complexities, e.g., the influence of terrain, gauge density, model forcings, climate variability, and uncertainties in hydro-climatic variables on drought characterization (meteorological, agricultural, hydrological), statistical rotation is emerging as useful and innovative contemporary methods (see, e.g., Agutu et al., 2020, 2017, Montazerolghaem et al., 2016, Kurnik et al., 2015).

In this study, a novel two-step regularization procedure that combines cumulant rotation (Ziehe, 2005, Cardoso, 1999, Cardoso and Souloumiac, 1993) with support vector machine regression (SVMR, Vapnik, 1995) is employed to assess and identify hydrological regions in Brazil where extreme events (floods and droughts) have been associated with indices of oceanic variability such as El-Niño Southern Oscillation (ENSO) and Pacific Decadal Oscillation (PDO) among others (e.g., Erfanian et al., 2017). Indeed, science must take the lead in providing information and evidence and strive to enhance an unequivocal understanding and visualization of relevant conditions (Sullivan, 2011). It is on this premise that this study specifically seeks to (i) characterize spatial and temporal variability of drought evolution based on meteorological and land water storage data, (ii) provide information on drought statistics and characteristics on different spatio-temporal scales, and (iii) identify regions where drought events are considerably associated with climate tele-connection patterns in order to understand the complexities and interactions of climate with freshwater availability. The use of indicators, be it in the context of human development, water management and governance, environmental assessment or even economic policy is well known. With this in mind, the World Meteorological Organization (WMO) recommended SPI is employed for drought characterisation and its long-term statistics. While SPI is widely used because of its ability to ensure a more useful and consistent interpretation of drought events for practical purposes, reanalysis data is also introduced in drought assessment over Brazil for the first time to assess its potential as a suitable metrics to identify influence of global climate on temporal drought patterns. More details about the data and method used are indicated in subsequent sections.

2. Materials and method

The methodological framework and work flow, including the data used in this study are summarised in Fig. 2.

2.1. Study region

Brazil, a country covering the north and south hemispheres within a latitude band ranging from 5° N to 34° S (Fig. 1), has approximately 8.5×10^6 km^2 ranking as the world's fifth-largest country by area. About 60% of Brazil lies within the tropics because of its shape and due to its latitude range and physiography, there is strong variation in climate across the north-south band. The Kopen climate types of Brazil consist of rainforest (Af) at the northwest; monsoon (Am) at the central Amazon; savanna (Aw), which covers the Brazilian Plateau over most of

the eastern, southern and central portions of the country; hot semi-arid (BSh) covering a large part of northeast Brazil; humid subtropical (Cwa) and subtropical highland (Cwb) over the southeast; and humid subtropical (Cfa) and oceanic (Cfb) over the south. Figure 1b shows that on the average, annual temperature decreases gradually from about 28°C in the north to about 18°C or less in the south of the country. Annual averaged rainfall varies from 500 to 3500 mm (Fig. 1a) with most rainfall occurring during the austral summer (December and April). The Northeast region is notoriously dry and it contrasts with the rest of the country (Fig. 1a). The mean annual rainfall in Northeast Brazil is less than 800 mm and the region is a scenario of severe drought events that are correlated with El Niño years. The Brazilian Plateau has annual precipitation ranging from 1000 to 2000 mm with a dry season from June to August. The South and Southeast Brazil also present high amounts of annual rainfall with values reaching up to 2000 mm per year. The quantity of annual precipitation over the Amazon region reaches amplitudes as high as 3000 mm per year (Fig. 1a), in which dry season generally lasts up to five months.

Figure 1a shows the mean values of the annual accumulated rainfall at which a ridge is seen from northwest-southeast across southeast Brazil into the southwest Atlantic Ocean, which is mainly due to the Brazilian highlands (plateau) and South Atlantic convergence zone (SACZ). The SACZ is strong in warm seasons and weak or nonexistent during the cold seasons. The increase of humidity in South Brazil supports the SACZ when the country warms up and generates the advection of moisture from the Atlantic to the Amazon by the low-level jet stream (LLJ), which feeds convective rainfall over the sub-tropical plains in South America. Furthermore, the Bolivian high, an upper-level (approx. 200 mb) anticyclone, contributes to the intensification of the SACZ during austral summer impacting, for example, Southeast Brazil with heavy rainfalls. Another wet belt evident in Fig. 1a is due to the intertropical convergence zone (ITCZ) that produces the highest precipitation over the western Amazon basin and near the mouth of its river (Amazon River). Furthermore, rainfall anomalies in this regions also presents correlations with SST where its warm condition to the north of the equator (Figs. 1a-b) leads to enhanced convection in the ITCZ, brings drought to Northeast Brazil and, conversely, when the warm anomalies lies to the south of the equator the position of the ITCZ causes above-normal rainfall in the region. Despite the plenitude of rainfall, droughts have also occurred in the Southeast (e.g., $2014 - 2015$) and Amazonia (2005, 2010, 2016) areas of Brazil.

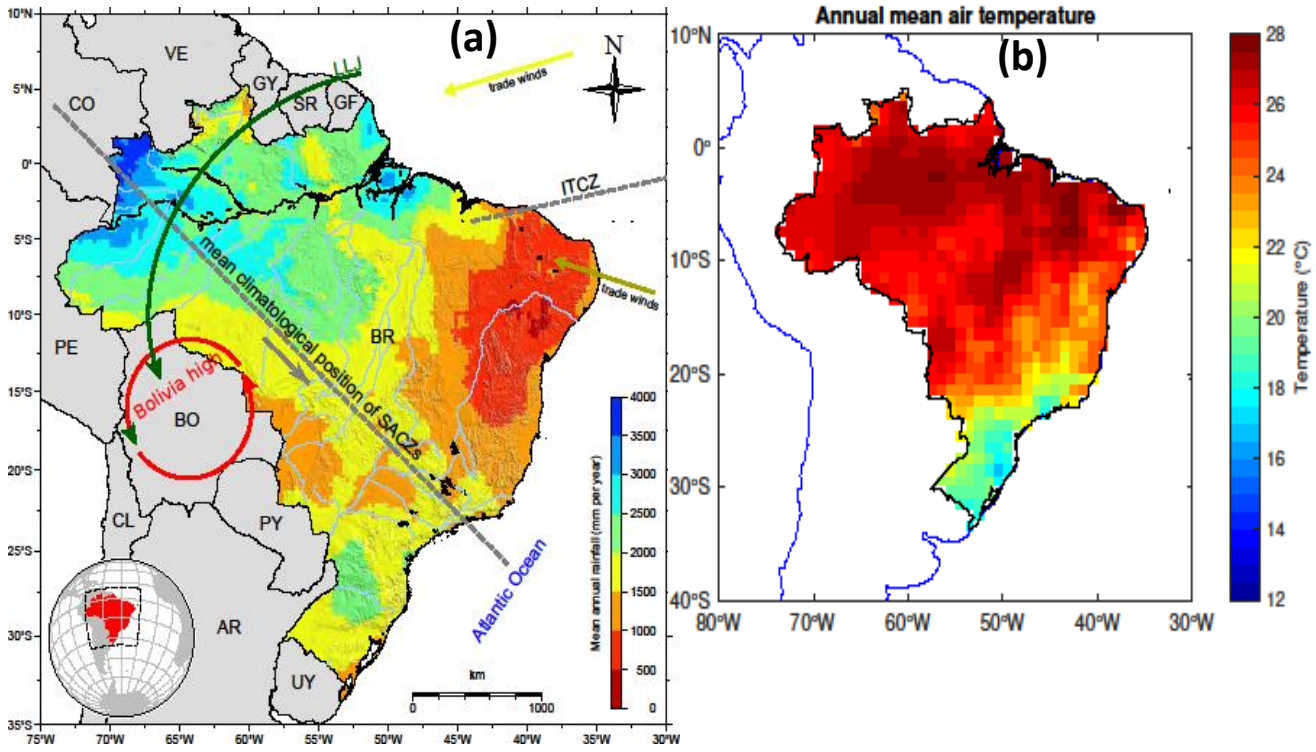

Figure 1: Study area showing mean annual distribution of (a) rainfall and (b) over Brazil. Surface temperature was computed based on GLDAS-Noah version 2.0 (https://disc.gsfc.nasa.gov/datasets/GLDAS_NOAH10_M_2.0/summary) during the January 1980 to December 2014 period.

2.2. GPCC-based Precipitation

The Global Precipitation Climatology Centre (GPCC) precipitation data (Schneider et al., 2014) was used to construct the standardised precipitation index (SPI) used in this study. GPCC provides reliable monthly gridded data sets of global land-surface precipitation and is a well known reference precipitation data because it has the largest gauge-observation data available globally. The 0.5 ° x 0.5 ° GPCC precipitation was downloaded from the GPCC data portal (www.ftp.dwd.de/pub/data/gpcc/html/downloadgate.html) and covers the period between 1980 and 2015. As a widely used observational reference data, it was found suitable drought characterization in East and West Africa and consistent with Climate Research Unit (CRU) observations over the Congo basin (e.g., Ndehedehe et al., 2020, Agutu et al., 2017).

2.3. MERRA land water storage

Modern-Era Retrospective Analysis for Research and Applications (MERRA) National Aeronautic and Space Administration (NASA) global high-resolution MERRA reanalysis data (Rienecker et al., 2011) was also use in drought analysis. The MERRA data is a state-of-the-art reanalysis land water storage that provides atmospheric fields, water fluxes, and global

estimates of soil moisture (Rienecker et al., 2011). Although it excludes canopy water content, outputs from MERRA have been used in the study of agricultural drought assessment, and climate teleconnections in the African continent (e.g., Agutu et al., 2017, Ndehedehe et al., 2017) and has been evaluated and recommended for land surface hydrological studies (e.g., Jung et al., 2017, Reichle et al., 2011). The land TWS data component of MERRA used in this study, covers the period of $1980-2015$ at $0.5°$ latitude by $0.625°$ longitude and is available for download through NASA's website (http://disc.sci.gsfc.nasa.gov/mdisc/).

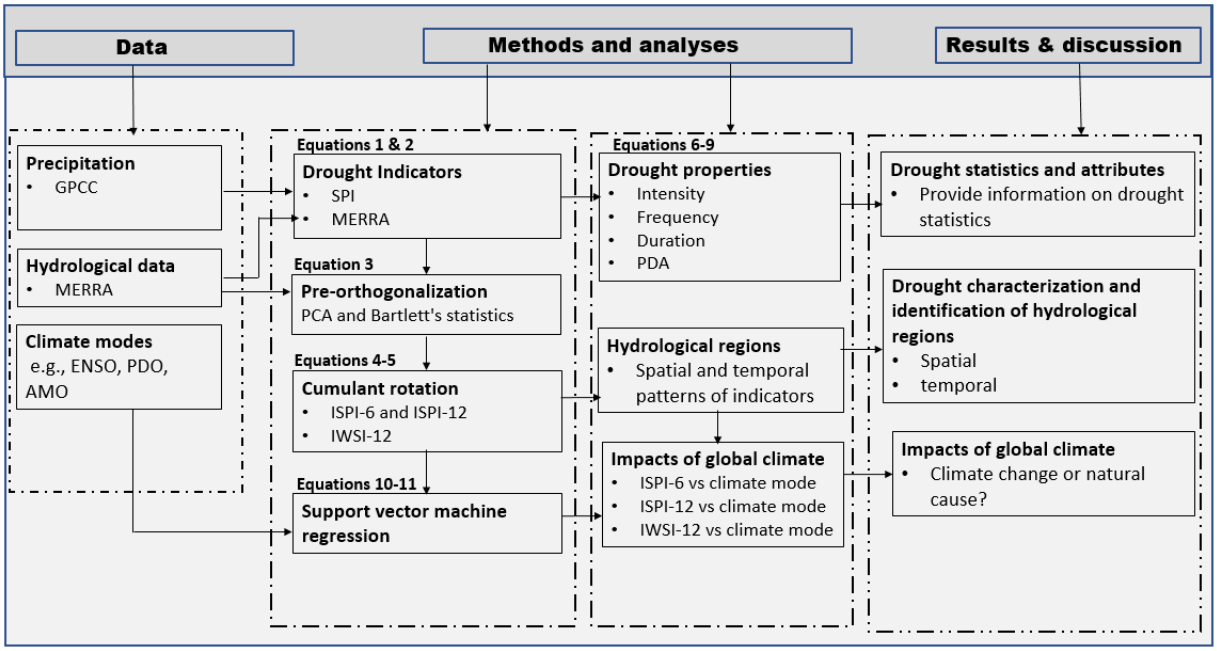

Figure 2: A schematic representation of the work flow used in this study. Specific details on data processing, analytical procedures, and implementation of equations 1-10 are provided in Section 2

.

2.4. Global climate variability indices

To identify hydrological hot spots in Brazil the relationship of localised drought indicators with several prominent indices of oceanic variability was explored. These climate variabilities include, El-Niño Southern Oscillation (ENSO), Indian Ocean Dipole (IOD), Atlantic Multi-decadal Oscillation (AMO), Atlantic Meridional Mode (AMM), Pacific Decadal Oscillation (PDO), Quasi-Biennial Oscillation (QBO), and Maiden Julian Oscillation (MJO). These datasets were downloaded from NOAA's data portal (`http://www.ncdc.noaa.gov/teleconnections`). Over South America, the influence of these climate teleconnections on land water storage and extreme droughts and water deficit conditions have been reported (e.g., Ndehedehe and Ferreira, 2020b, Erfanian et al., 2017, Sun et al., 2016, de Linage et al., 2014).

As with other regions, interannual climate variability in Brazil is associated with the occurrences of, among other factors, the El Niño (warm condition) and La Niña (cold condition) phenomena. El Niño episodes are generally associated with below-normal rainfall in northern Brazil and above-normal conditions in southern Brazil. Conversely, rainfall anomalies in both regions are usually observed during La Niña events. This generalization of ENSO-related anomaly in rainfall regimes could vary while analyzing its impact at regional to local scales in Brazil. For instance, the droughts of northeast Brazil are generally recognized when El Niño conditions take place in the tropical Pacific (e.g., Marengo et al., 2018, Erfanian et al., 2017). As the mesoscale convective systems, physical and other atmospheric mechanisms and teleconnections that drive precipitation differ across continents and regions, the role of these teleconnections on drought properties and evolutions are examined for Brazil, which is home to the Amazon basin. Further description of these climate modes and how they were generated are available on NOAA's online data repository.

2.5. Empirical probability-derived drought indicators

As with several other aspects of human development, environmental sustainability and performance, quantifying drought can easily be achieved through the use of indicators and metrics (e.g., Ndehedehe et al., 2020). Drought-related stress arising from precipitation deficits (meteorological), limited soil moisture (agricultural) and abnormally low water levels, in lakes, reservoir levels, and groundwater (hydrological) can be studied using several drought indicators. These indices/indicators are crucial for understanding water availability and the assessment of different drought intensities (meteorological, agricultural and hydrological) on a broad range of scales. In this study, drought indicators (SPI) at 6 and 12 month cumulation (agricultural and hydrological) were based on the GPCC-derived standardised precipitation index (SPI, McKee et al., 1993). The need for a comprehensive drought monitoring system that provides accurate drought statistics and early warning, led to *The Lincoln Declaration on Drought Indices* to unanimously adopt SPI and recommend same to WMO as a standard index to track and characterize various levels of drought events (Hayes et al., 2011). Our use of SPI in this study was mainly driven by this consensus and the fact that it is now widely used and a recommended drought index by WMO for meteorological and hydrological drought assessment, in addition to other less popular drought indicators. Depending on the hydrological response of some semi-arid regions to rainfall conditions, 6-month cumulation can be used to assess impacts of rainfall deficits on hydrological stores such as soil moisture and

groundwater. Hydrological processes are complex in some regions and drought impacts and its cascading effects could be difficult to understand because of local climatic influence or land surface conditions. Consequently, the MERRA data is synthesized after the similitude of SPI and is also introduced as a drought indicator over Brazil. These indicators including, that the MERRA data use an empirical probability method, pioneered by Hao and AghaKouchak (2014) to derive a non-parametric standardised index as,

$$p(x_j) = \frac{m_j - 0.44}{n + 0.12}, \tag{1}$$

where n is the sample size, i represents the rank of non-zero precipitation data starting from the smallest while $p(x_j)$ is the corresponding empirical probability. Eqn 1 is transformed to a standardised index as (Farahmand and AghaKouchak, 2015)

$$SI = \phi^{-1}(p) \tag{2}$$

where ϕ is the standard normal distribution function and p is the probability obtained from Eqn. 1. Drought classification and the various drought intensities (extreme, severe, and moderate) during the period and their aerial extent were estimated based on the thresholds described in McKee et al. (1993), which assumed that a drought condition occurs when the drought index is consistently negative and reaches a value of -1. A drought event ends when the SPI becomes positive. For every drought event, there is a duration, which is defined by its beginning and end. Drought magnitude is the positive sum of the SPI values for all the months within a drought event. The use of SPI in this study as an appropriate indicator is motivated by the recommendation of WMO and the assumption that drought is primarily driven by precipitation deficits (e.g., Ndehedehe et al., 2020, Spinoni et al., 2014). However, given that strong land-atmosphere interactions could slightly interfere with drought intensities and the propagation of droughts in some regions, the same empirical probability method is employed to standardise the MERRA data similar to GPCC.

2.6. Two-step regularization approach for spatial and temporal regionalization of hydrological indicators

A two-step regularization approach was employed to localise empirically-derived drought indicators. To this end, the gridded time series of computed drought indicator ($\mathbf{X}$) at 6 and 12 month scales were decomposed into temporal and spatial patterns using the principal component analysis (PCA, e.g., Jolliffe, 2002). Given a centered matrix of SPI values as $\mathbf{X}$= $[x(p_k, t)]$ where p_k is space locations; k = 1, 2, . . ., Nx, which are the number of spatial

locations for $\mathbf{X}$, and t is the time (monthly) step from $1980-2014$. The technique decomposes the fields $\mathbf{X}$ into spatial and temporal series as,

$$\mathbf{X}(t) = \sum_{k=1}^{N} a_{(k)}\mathbf{p}_k \tag{3}$$

where $a_{(k)}$(t) are the temporal series also called expansion coefficients (or sometimes standardised scores) and $\mathbf{p}_k$ are the corresponding spatial patterns (empirical orthogonal functions-EOF loadings). Although this tool as been broadly employed in the regionalization and spatio-temporal analysis of geophysical time series and drought patterns globally (e.g., Ndehedehe et al., 2020, Agutu et al., 2017, Montazerolghaem et al., 2016, Santos et al., 2010), this technique serves primarily as a regularization tool to minimize and filter the noise and random signals in the data and the Bartlett's test statistics (Snedecor and Cochran, 1989) was employed to ensure that random variations from the PCA scheme were not retained. Notably, the process of retaining significant modes of variability from this scheme can vary from, e.g., rules based on hypothesis testing to subjective choices (e.g., *log-eigenvalue* diagram and retaining PCs that represent a 'sufficient fraction'of the variance in the original data) depending on the purpose of the statistical decomposition (see, e.g., Wilks, 2011, Martinez and Martinez, 2005). Our choice of Bartlett's test statistics for Brazil was sufficient for the pre-orthogonalization stage (step 1). In the second stage after the data has been pre-orthogonalized, a classical rotation towards statistical independence based on the fourth order cumulant matrices was performed to localised all drought indicators at 6 and 12 month aggregation scale. These cumulants provide the suitable matrices to be diagonalized before a rotation towards statistical independence. The algorithm used to rotate the PCA-regularised data matrix $\mathbf{X}$ is detailed in pioneering works of Cardoso and Souloumiac (1993) and Cardoso (1999). This algorithm is computationally efficient and exploits key remote properties of the signals, such as non-Gaussianity and uses the Joint Approximate Diagonalisation of Eigen matrices (JADE) approach (Ziehe, 2005, Cardoso, 1999, Cardoso and Souloumiac, 1993). From the JADE algorithm, the fourth-order cumulant tensor provides the suitable matrices to be diagonalized, which are non-gaussian (see, e.g., Cardoso, 1999, Ziehe, 2005):

$$\mathbf{C}_{i,j}(\mathbf{M}) = \sum \; cum(x_i, x_j, x_u, x_v)\mathbf{M}_{u,v}, \tag{4}$$

such that $\mathbf{M}$ is an arbitrary matrix. After the eigen decomposition of the centered covariance matrix x, an approximate joint diagonalisation of the set of eigen matrices of the cumulant tensor with an orthogonal transformation, which comprises a sequence of plane rotations is

then implemented by the JADE algorithm (see, e.g., Ndehedehe et al., 2016, Ziehe, 2005, Cardoso and Souloumiac, 1993). For interested readers, this cumulant-based methods have been described in detail with further numerical steps and mathematical formulations available (Theis et al., 2005, Common, 1994, Cardoso and Souloumiac, 1993, Cardoso, 1999). Through a contrast optimization by the joint diagonalization approach, the rotated cumulant matrices resulted in well localised spatial patterns (ISPI and IWSI) **S**, and temporal patterns **A**, as: (e.g., Ndehedehe and Ferreira, 2020a)

$$\mathbf{R}_{SPI/MERRA}(x, y, t) = \mathbf{AS}, \tag{5}$$

where $\mathbf{R}_{SPI/MERRA}$ is the rotated drought indicator, (x, y) are pixel locations, t is the monthly time step. **A** is also known as independent components, which is unit-less since it has been normalised using its standard deviation while the corresponding spatial patterns **S**, have been scaled using the normalised independent components (i.e., **A**). The spatial and temporal patterns of SPI at 6 and 12 month cumulation were localised over Brazil using the cumulant decomposition method. The classification scales (e.g., extremely wet, moderately dry, severely dry, extremely dry) for the SPI values (hereafter independent standardised precipitation index ISPI for the spatial patterns) are jointly derived from each independent mode (i.e., spatial and temporal patterns). This statistical decomposition enables the identification of extreme climatic hot spots (droughts) in the region.

2.7. Drought statistics and characteristics

Drought properties including, the duration, frequency, intensity and distribution of affected areas (see, e.g., Diaz et al., 2019, Wang et al., 2018, Mao et al., 2017, Spinoni et al., 2014) are determined for each drought event during the study period ($1980 - 2015$). The prediction of areas under drought following the method of Diaz et al. (2019) allows estimation of drought-affected areas and the visualization of outcomes in space and time as opposed to previous studies (e.g., Agutu et al., 2017). The integration of SPI time series events into aggregated areas of drought, and the subsequent estimation of the percentage of drought area (PDA) for each time scale and step is computed as (Diaz et al., 2019)

$$PDA = \frac{100}{A_r} \sum_{c=1}^{N} (d_s(t) * A), \tag{6}$$

where where A is the area of the cell c and A_r is the region area, t is time step, d_s, drought state and the magnitude of drought is the PDA value. In this study, drought duration is defined as

the time length (i.e. the number of months) between the drought onset and termination (e.g., Mao et al., 2017, Spinoni et al., 2014). It is calculated by the sum of durations for all drought events divided by the number of drought events (e.g., Haile et al., 2020, Xu et al., 2019) as

$$D = \frac{\sum_{i=1}^{n} d_i}{n}, \tag{7}$$

where D is the drought duration (months), d_i, duration of ith drought event, and n the total number of drought events. Drought frequency refers to the number of drought occurrences in a given time period (Yu et al., 2014). It is estimated as the ratio between the number of drought months and the total number of months in the time series (e.g., Wang et al., 2018, Spinoni et al., 2014) as

$$F = \frac{n_m}{N_m} \times 100, \tag{8}$$

where F drought frequency (%), n_m, the number of drought months, and N_m the total number of months. Drought intensity measures drought severity per its duration useful to inform the strength of droughts (Zhang et al., 2015). It is the absolute value of the average of accumulated SPEI values during the drought events and is computed as (e.g., Haile et al., 2020, Wang et al., 2018)

$$I = \mid \frac{1}{n} \sum_{i=1}^{n} SPI_i \mid, \tag{9}$$

where I is drought intensity (-), n = number of drought occurrences in months, SPI_i, is SPI value below the threshold (–1). For each duration of the drought event, drought severity measures the cumulative deficit below the truncation level to quantify drought intensity (Zhang et al., 2015).

2.7.1. Oceanic hot spots associated with temporal drought patterns

To understand the influence of global climate on hydrological hot spots, the support vector machine regression model (SVMR, Vapnik, 1995) was employed. The support vector machine (Cortes and Vapnik, 1995) algorithm was extended by Vapnik (1995) for regression using an ε-insensitive loss function. The SVMR concept is based on the computation of a linear regression function in a high-dimensional feature space in which the input data (x_i) are mapped through a non-linear function (e.g., Okwuashi and Ndehedehe, 2017). This mapping is warranted because most of the time, the relationship between a multidimensional input vector x and the output y is unknown and could be non-linear (e.g., Wauters and Vanhoucke, 2014). A two-step procedure is adopted in the implementation of the SVMR scheme. Finding a linear hyperplane that fits the multidimensional input vectors to output values is the first step, thereafter, the

SVMR predict future output values that are contained in a validation set (e.g., Okwuashi and Ndehedehe, 2017, Wauters and Vanhoucke, 2014, Smola and Schölkopf, 2004, Vapnik, 1995). Assuming the set of data points $\mathbf{X} = (x_i, p_i), i = 1..., n$ with x_i being the predictand data point i, p_i the actual value and n the number of data points. The linear SVMR function $f(x)$ takes the form (e.g., Vapnik, 1995)

$$f(x) = wx + b. \tag{10}$$

The assume linear parameterization in Eqn 10 above bears similarity to a linear regression model. That is because the predicted value, $f(x)$, depends on a slope w and an intercept b. However, The goal of the SVMR is to identify a function f(x) that has a maximum deviation ε from the target values p_i and has a maximum margin for all training patterns x_i. In order words, a balance between learning the relation between inputs and outputs whilst maintaining a good generalization behavior is targeted. As highlighted further in Wauters and Vanhoucke (2014) too much focus on minimizing training errors may lead to overfitting. Hence, a pre-specified penalty value (C) is introduced as a trade-off to create the balanced between generalization and good training. That is, C regulates the trade-off between the regularization term ($\frac{1}{2} \parallel w \parallel^2$) and the training accuracy in the formulation below as (e.g., Wauters and Vanhoucke, 2014, Vapnik, 1995),

$$\zeta = \frac{C}{n} \sum_{i=1}^{n} L_\varepsilon(p_i, f(x)) \frac{1}{2} \parallel w \parallel^2, \tag{11}$$

where the compound risk caused by training errors and model complexity is given as ζ. Eqn. 10 provides the estimated values for w and b and comprises the empirical risk measured by the ε-insensitive loss function, L_ε and the regularization term $\frac{1}{2} \parallel w \parallel^2$, which describes the model complexity (Wauters and Vanhoucke, 2014, Cortes and Vapnik, 1995). Specifically, a linear SVM regression model was trained to fit the data. The SVMR technique evaluates each run of the experiment using regression, by partitioning the data internally into training, validation, and testing components (i.e., 55% of the total data). The remaining 45% of the observed data were thereafter used for forward prediction based on the hold-out method of cross-validation (e.g., Haley, 2017). The stratified partitioning of the data using this approach ensures that each partition includes similar amount of observations from each group. Further, the relationship of climate teleconnections and drought indicators are assessed using Pearson correlation and coefficient of determination (R^2).

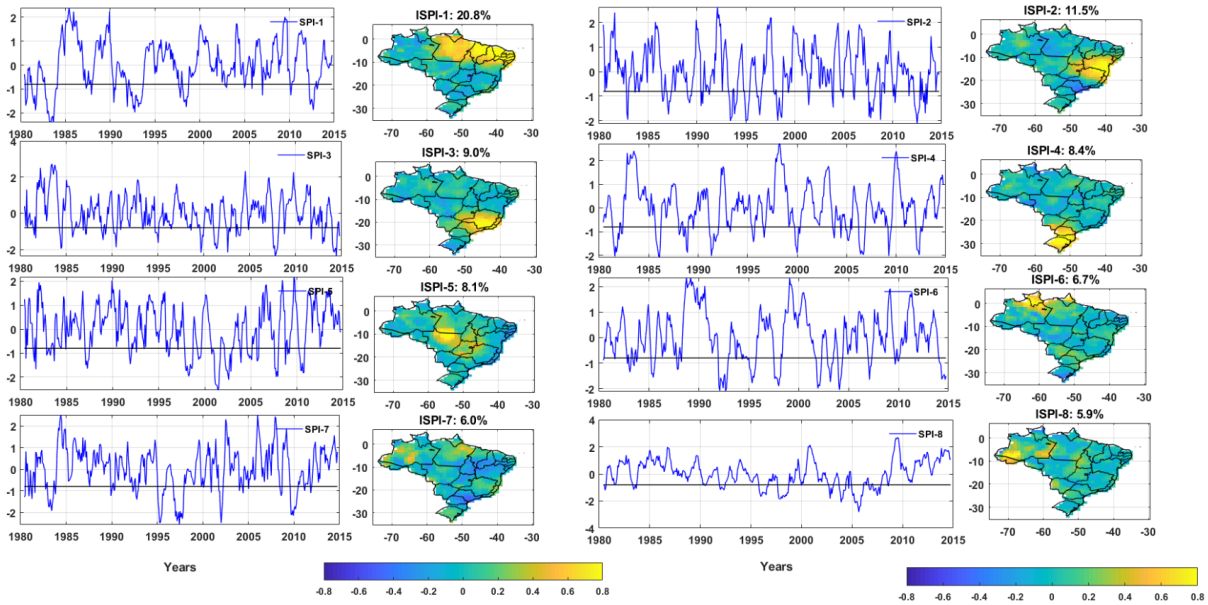

Figure 3: Spatial and temporal independent standardised precipitation index (ISPI) patterns over Brazil using 6-month SPI values. SPI values are computed using GPCC-based precipitation for the period between 1980 and 2015. Actual values for drought classification and categorization with respect to McKee et al. (1993) description are jointly derived from the regionalised spatial patterns (first and third columns) and their corresponding temporal evolutions (second and fourth columns). The black solid line is the drought threshold.

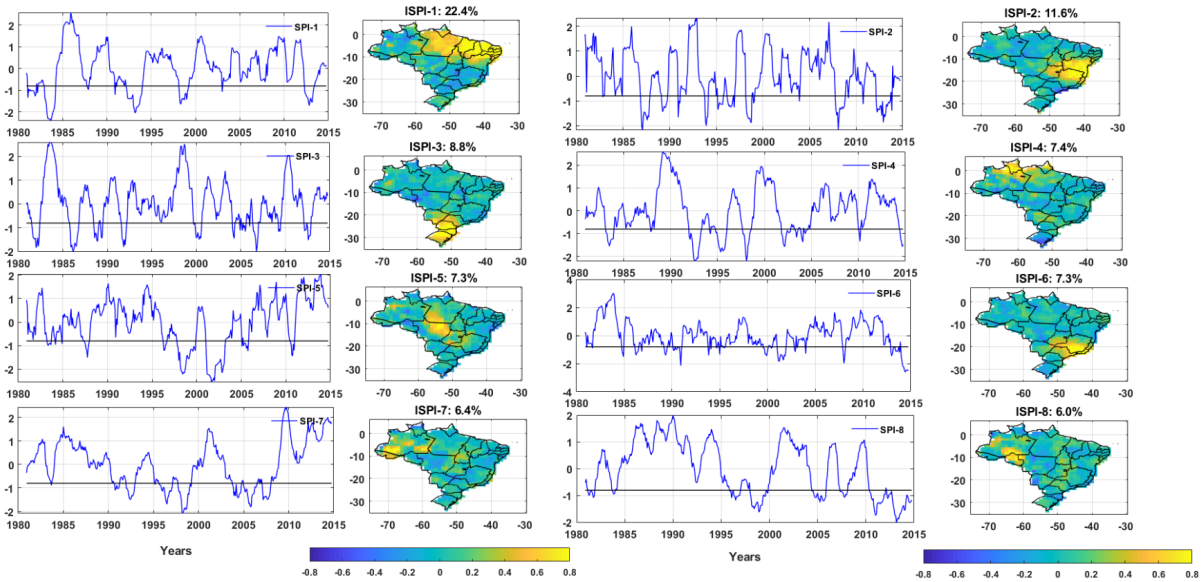

Figure 4: Same as Fig. 3 above but using 12-month SPI values.

3. Results

3.1. Regionalization of hydrological hotspots through pre-orthogonalization

Well localised spatio-temporal patterns of drought indicators (ISPI and IWSI) were identified through a classical rotation of the pre-orthogonalized SPI data matrices towards statistical

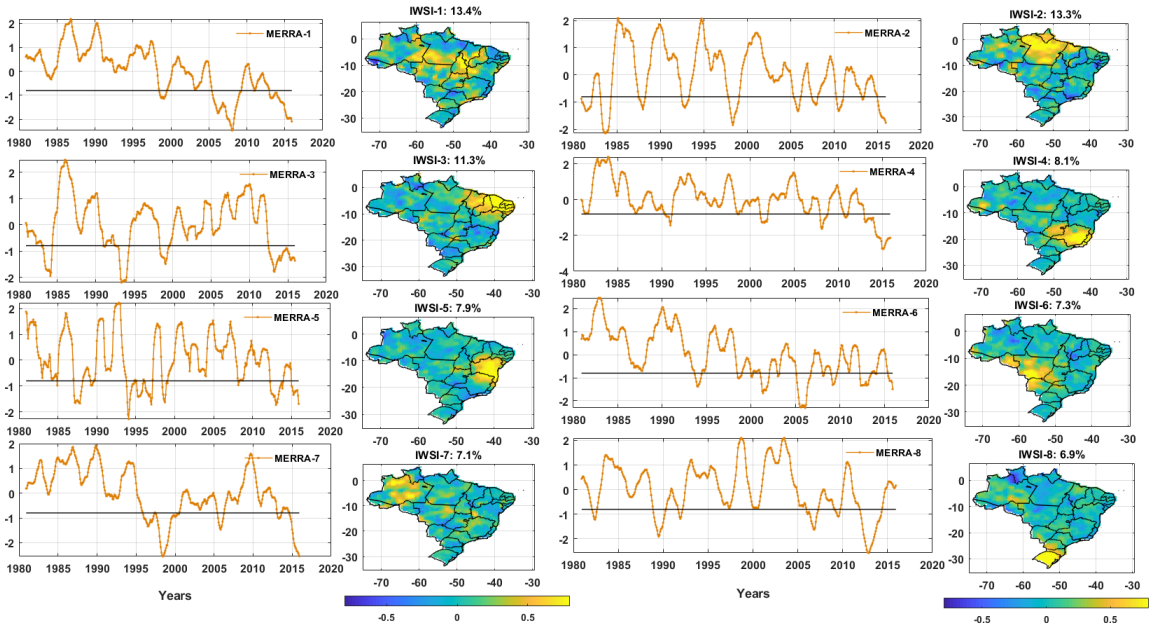

Figure 5: Spatial and temporal MERRA-SPI patterns over Brazil using 12-month aggregation. MERRA-SPI implies that the MERRA indicator values are computed similar to SPI for the period between 1980 and 2015. The black solid line is the drought threshold.

independence using the cumulant method (Figs. 3-5). Previous approaches to spatio-temporal drought analysis relied on component extraction techniques (e.g., Agutu et al., 2017, Bazrafshan et al., 2014). But the regionalization of drought indicators as implemented here leverages on the fourth order cumulant of the data matrix based on remote properties that include, non-Gaussianity, spectral non-Flatness, and non-stationarity (e.g., Theis et al., 2005, Cardoso and Souloumiac, 1993, Cardoso, 1991) and is different from other fixed-point iteration schemes employed in the decomposition of gravity observations and geological objects identification (e.g., Yang and Cheng, 2015, Frappart et al., 2011). This method resulted in the localization and extraction of physically meaningful and independent spatial patterns of drought indicators. The localised spatial patterns (ISPI and IWSI) over Brazil are captured in eight independent patterns (temporal and spatial) and represent hydrological hotspots with significant variability in SPI during the $1980 - 2015$ period.

Regardless of the time scales, the spatial patterns of localised drought indicators based on the cumulant rotation are consistent (Figs. 3-5) even though there are slight differences in the total variabilities accounted for in their independent modes. Be it 6 or 12 month cumulation, SPI spatial patterns over Brazil are localised over the north, north-east, south, south-east, central and north-west regions. Drought variability is higher in the extreme north accounting for 20.8% and 22% in SPI-6 and SPI-12, respectively (SPI-1, Figs. 3-4) compared to other

regions. It is noted that drought events in the most humid regions (the Amozon catchments) are less frequent and accounts for little variability in the observed SPI and MERRA indicators unlike the strong climatic hot spots in the north/north-east sections (Figs. 3-5 and cf 1). However, the spatial patterns of drought indicator based on MERRA (IWSI) appear to be slightly different except for some key areas (e.g., north, south and north-east Brazil) that are consistent with the localised spatial patterns of ISPI (Fig. 5). Different from the SPI indicators, areas along central Brazil (mostly the Amazon) show strong decline in IWSI since 1980 and specifically highlights the major drought events that ravaged the Amazon region (MERRA-1/IWSI-1, Fig. 5). While the MERRA indicator also revealed the drought events between 2000 and 2015 in south-west Brazil (MERRA-6/IWSI-6, Fig. 5), the most humid part of Brazil (cf. Fig. 5) was also affected by the prominent drought events of 1998/1999, 2005, and $2012-2015$ period (MERRA-7/IWSI-7, Fig. 5). Given that rainfall only provides an indirect observation of water availability (e.g., Chen et al., 2014), some of these differences between SPI and MERRA indicators would be expected. This is because of the intrinsic hydrological response of surface hydrology and land surface conditions in some semi-arid/or moderately humid regions to extreme climate events such as droughts.

As would be expected, drought frequency (number of events from the temporal evolutions) in all hydrological hotspots tend to be higher at 6 month cumulation (Fig. 3) compared to 12 month cumulation (Fig. 4). The regionalization of SPI over Brazil confirms that the occurrence of severe and extreme drought conditions vary in time and space. For example, temporal drought evolutions in northern Brazil significantly contrast with the southern section of the country (ISPI-1 and ISPI-4, Fig. 3). However, drought frequency tend to reduce at 12 month scale but with longer duration (Fig. 4). But the spatio-temporal variability of drought event is again obvious (ISPI-1 and ISPI-3, Fig. 4), confirming that the influence of strong spatial variability in rainfall at all temporal scales and inter-annual climatological gradients across regions modulate drought magnitudes and its properties. This is true for north-east Brazil (ISPI-2, Fig. 4) where the number of drought events is relatively higher than other regions.

3.2. Drought characteristics and statistics

3.2.1. Percentage of areas under drought

To understand the impacts of droughts from a more holistic view, some statistics of drought characteristics are presented. These statistics are based on percentage of affected areas, drought duration frequency, and intensity. At the 6 and 12 month aggregation, evolution-

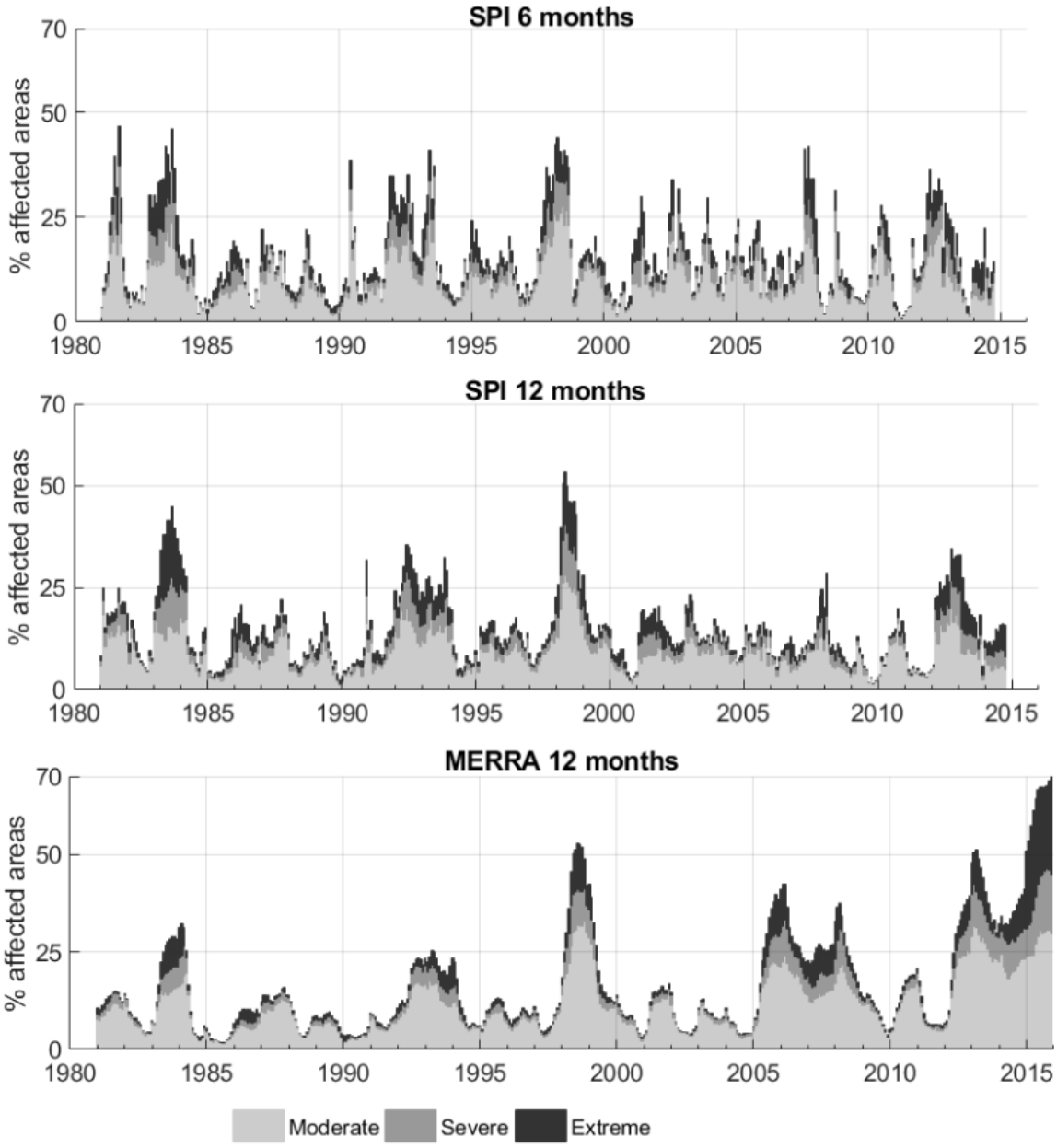

Figure 6: Areas under drought over Brazil for various drought intensities (extreme, severe, and moderate) during 1980-2015 period expressed in percentage (%). The affected areas are characterized based on SPI-6, SPI-12, and MERRA-12 months aggregation.

ary drought patterns of droughts in terms of their characteristics and intensities (moderate, severe, extreme) over Brazil have shown temporal patterns that are somewhat similar to the results in previous section. From the SPI indicator, key periods when areas affected by extreme drought exceeded 25% were the early 1982/1983, 1992/1993, 1998, and 2012/2013. The MERRA indicator show similar patterns but a bit exaggerated for the period between 2005

and 2010. The predominance of extreme drought events from SPI-12 and MERRA-12 drought indicators however, agree that more than 50% of Brazil was affected by the 1998/1999 drought (Fig. 6). Given Brazil's considerable dependence on hydroelectric power, Getirana (2016) noted that this drought (1998/1999) was the cause of the biggest energy crisis that ever occurred in the country. As the MERRA data extends to 2015, it has shown that one of the worst drought in recent times occurred during the $2012 - 2015$ period, fluctuating between 25% in 2012 and 70% in 2015 (Fig. 6). A comparative analysis of the three indicators (SPI-6, SPI-12, and MERRA-12) in their characterisation of various drought intensities and estimation of affected areas for specific drought periods (2007/2008, 2012/2013, and 2013/2014) show consistency between SPI-6 and SPI-12 month (Fig. 7a-c). However, there are significant differences in the predicted extents of affected areas from the MERRA indicator. This dissimilarity between the MERRA and SPI indicators in their estimated areas under drought are notable and varies during the three periods analysed (Fig. 7a-c). This might be attributed to difference in data sources (e.g., differences in MERRA precipitation rates). While rainfall is an indirect indicator of available water, the MERRA data accounts for total water held in all land surface reservoirs (e.g., soil moisture). If land surface processes, such as temperature, groundwater withdrawals for irrigation, and catchment characteristics influence drought propagation, these could have impacts on hydrological processes (e.g., infiltration and flow dynamics) and interactions between land surface-moisture fluxes and the atmosphere under an extreme drought scenario. MERRA-drought indicator therefore will be more reliable to capture these impacts because of the inclusion of soil moisture and latent heat flux in the model whereas precipitation-based drought indicator might be restricted.

In 2012, the predicted areas under drought by all indicators are rather close unlike in 2013 when the MERRA indicator shows considerable difference and contrast (Fig. 7b-c). Given the extreme drought condition of 2012/2013 period, this demonstrates the utility of MERRA indicator in capturing the cascading influence of droughts on soil hydrology and land water storage. The percentage of areas under drought showing the response of Brazil to drought events on both annual (January-December) and inter-annual time scales are indicated for all indicators (Fig. 8a-f). Most drought affected areas occurred in the months between April and October as was the case in 1982 and 1998. But areas affected by the 2015 drought in Brazil was phenomenal and is consistent with previous reports (e.g., Ferreira et al., 2018). The MERRA indicator shows this drought was an all-year (January-December) event with at least 60% areas under drought observed per month (Fig. 8e and f). Generally, all of these patterns are also

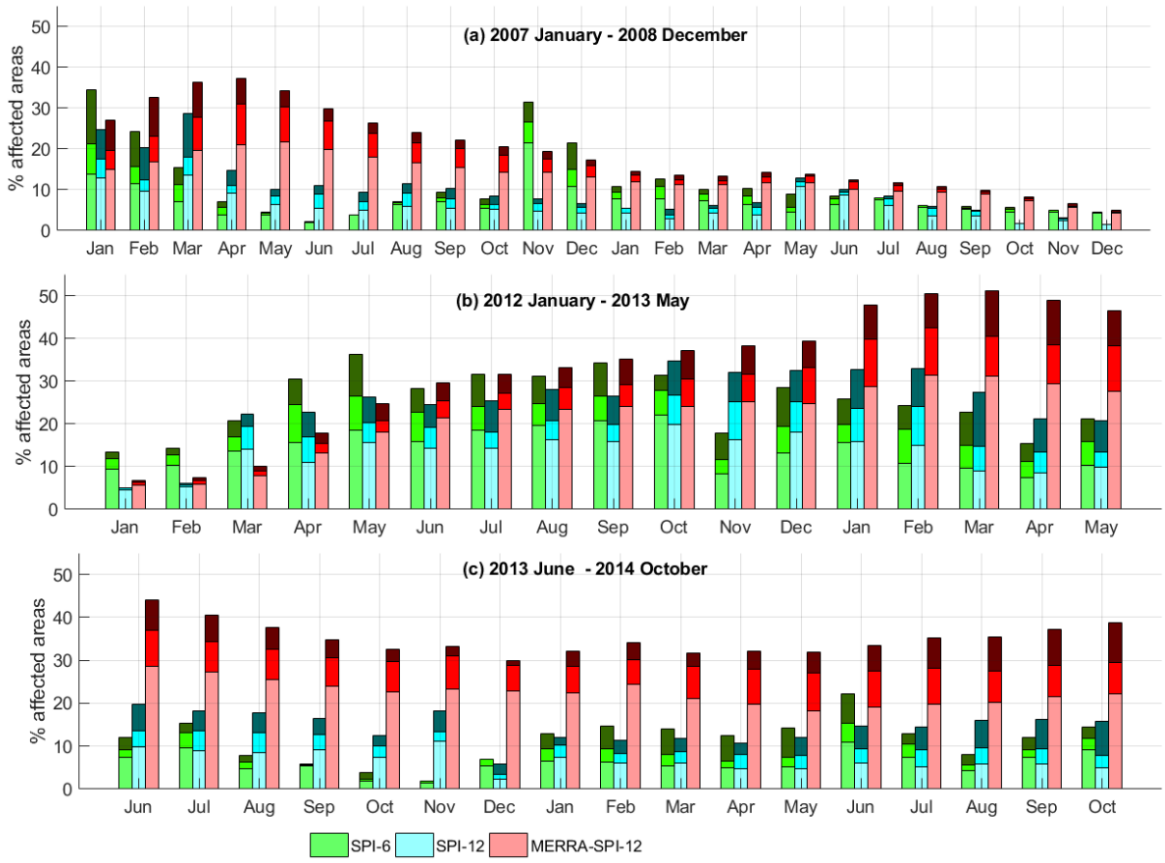

Figure 7: Areas under drought over Brazil similar to Fig. 6 above but only specific periods ($2007-2008$, $2012-2013$, and $2013-2014$) and is expressed in percentage (%). The affected areas are characterized based on SPI-6, SPI-12, and MERRA-12 months aggregation.

reflected in the yearly time series of percentage of areas under drought (Fig. 8b, d, and f).

3.2.2. Drought duration, frequency, and intensity

The spatial distribution of averaged drought properties (duration, frequency, and intensity) during the 1980-2014 period are summarised in (Figs. 9a-i). Drought duration is more extensive and wide spread on a 6 month (SPI-6) cumulation compared to 12-month (SPI-12) cumulation (Figs. 9a-c). A key observation is that the mean duration of drought episodes appear to be prevalent in around the Amazon and north-west sections of Brazil. The intrinsic response of these regions to limited rainfall is expected to be different because of their diverse climate feature. On a 12 month time scale, these regions tend to have longer drought duration, ranging from $8-10$ months compared to areas located on the south and north-east Brazil (Figs. 9b-c). Longer drought duration would generally be expected on a relatively higher cumulation scales (SPI-12) unlike shorter time scales (SPI-6). Although the MERRA indicator was also synthesize similar to the SPI-12, there is a significant difference in the mean duration of

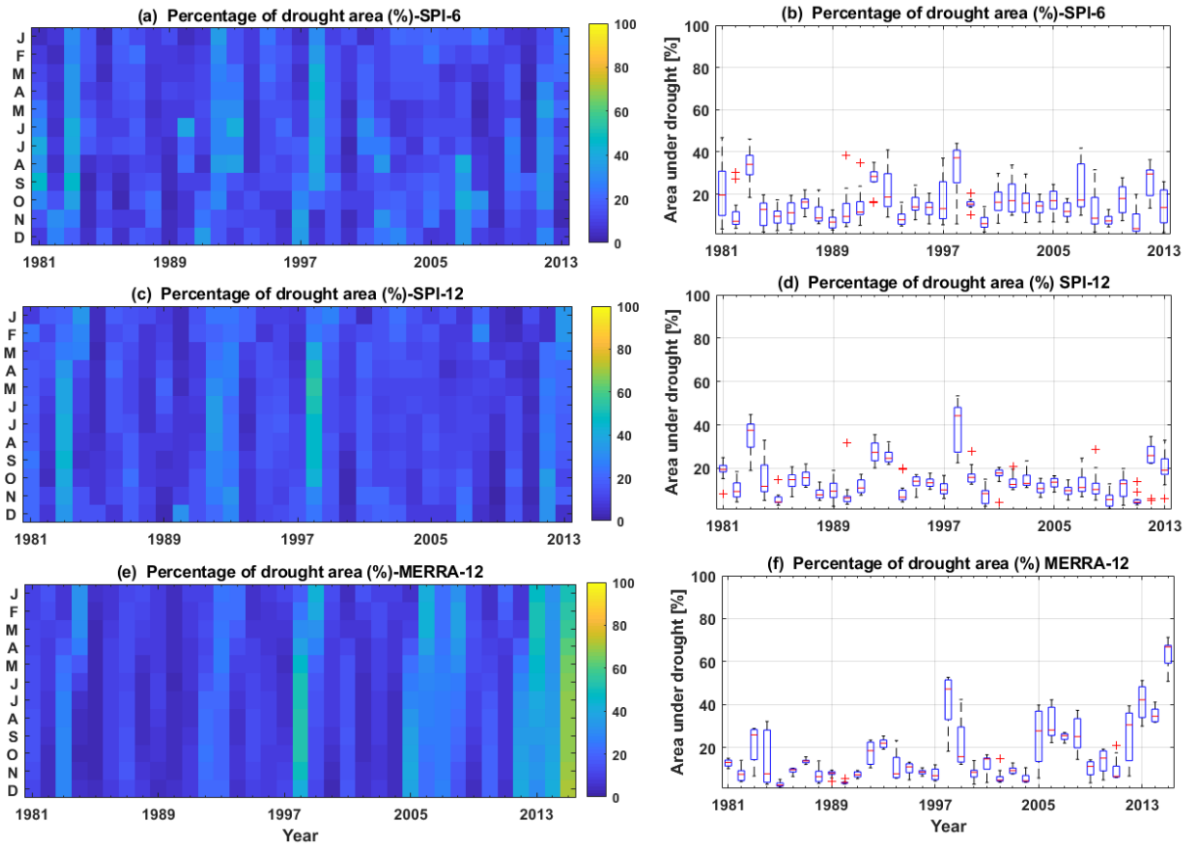

Figure 8: Averaged areas under drought for annual (a, c, and e) and inter-annual (b, d, and f) time scales over Brazil for the period between 1980 and 2014.

droughts quantified (Figs. 9b-c), especially in the south and north-east Brazil. Considering that rainfall is an indirect indicator of water availability, this difference can be embedded in the interactions of topography, soil characteristics, and vegetation with droughts or its propagation process under a rising temperature.

Estimated drought frequency tend to be much unique only for SPI-6 but similar for SPI-12 and MERRA indicators (Figs. 9d-f). The distinctiveness in the observed spatial patterns of drought frequency in Fig. 9d is consistent with the observed temporal evolutions of drought (SPI-6) in Fig. 3 where drought occurrence is relatively higher when compared to SPI-12 month temporal patterns (Fig. 4). Moreover, based on SPI-6, it is noted that drought is more frequent in the south of Brazil, ranging from 16% to 15.5% than some regions in the central and north-east sections where drought frequency is approximately between less than 15.5 and 14.5%. While drought is generally less frequent (slightly greater than 14.75%) when viewed from the spectacles of drought indicators with higher cumulation scales (12 month), there are few hot spots around the Amazon basin where it is even much less frequent and shows

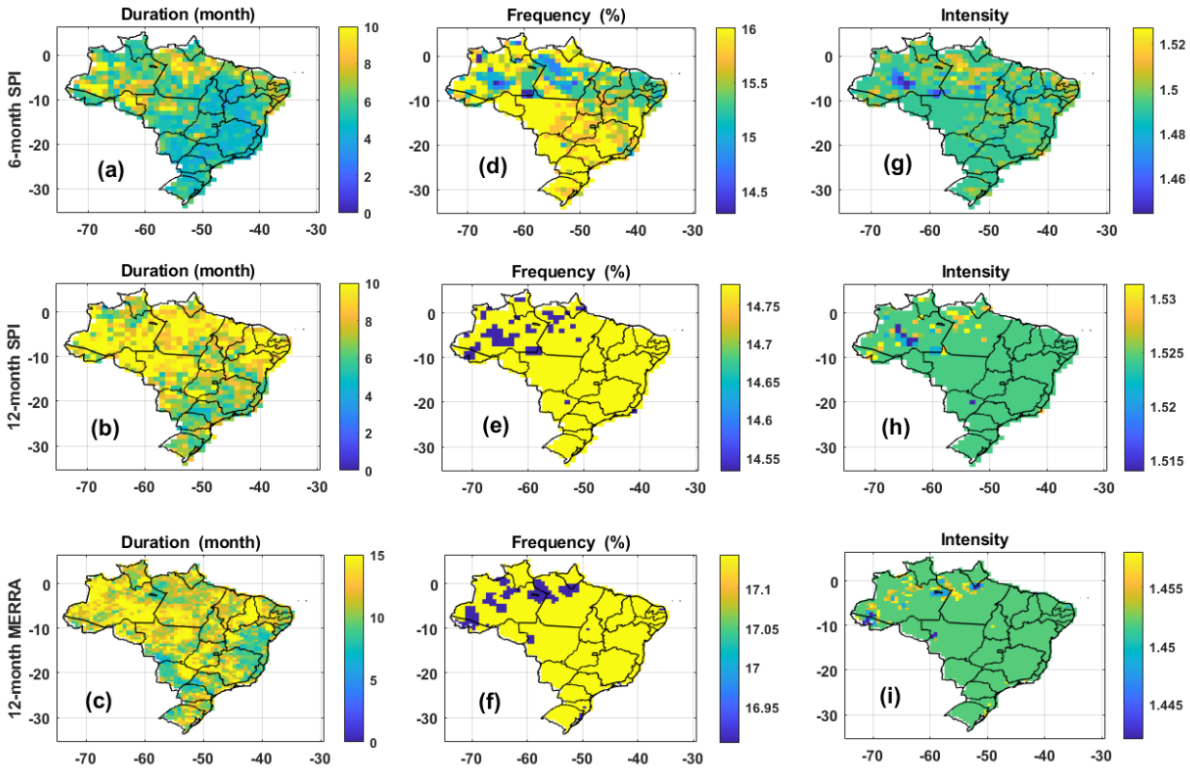

Figure 9: Estimated spatial distribution of drought (a-c) duration, (d-f) frequency and (g-i) intensity during the $1980-2014$ period (drought intensity is in standardised units.)

values less than 14.55% (Fig. 9e). But the spatial distribution of drought intensities shows they are fairly similar with large distributions of intensities ranging from 1.4 to 1.5 over Brazil regardless of time scales (Fig. 9g-i). In some regions however, especially at the shorter time scales, the distributions of intensities towards northern Brazil vary significantly.

3.3. Hydrological hotspots associated with multi-scale ocean atmosphere phenomena

The coupled variability of the temporal series of drought indicators associated with the hydrological hot spots (localised spatial patterns) identified in previous section with climate

Table 1: Relationship between observed and predicted drought indicator (SPI-12) in each hydrological region identified in Figs. 3-5 using all global climate teleconnection indices in Section 2.4 as predictors. Correlation values are statistically significant at $\alpha = 0.05$.

Region	ISPI-1	ISPI-2	ISPI-3	ISPI-4	ISPI-5	ISPI-6	ISPI-7	ISPI-8
SPI-6	0.52	0.28	0.15	0.40	0.32	0.49	0.46	0.43
SPI-12	0.36	0.46	0.35	0.53	0.31	0.42	0.26	0.54
MERRA-12	0.72	0.71	0.52	0.31	0.24	0.44	0.62	0.57

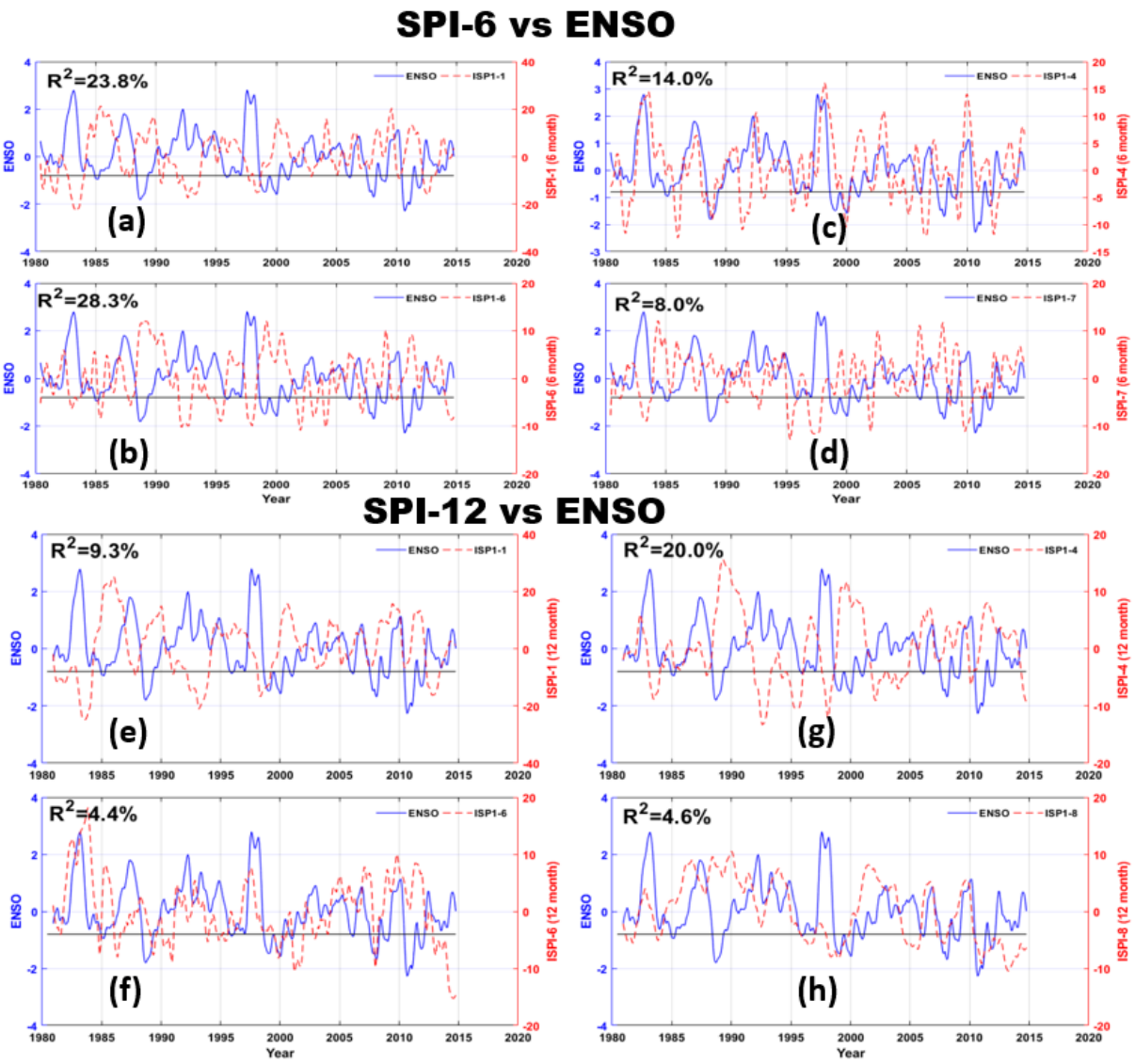

Figure 10: Influence of ENSO on evolutionary patterns of SPI. The relationship of ENSO with (a-d) SPI-6 month and (e-h) SPI-12 month are based on linear regression.

teleconnection patterns were assessed. Although this is a preliminary first step to evaluating the influence of multi-scale ocean atmosphere phenomena in these hot spots, we found considerable relationship between the time series of drought indicators with ENSO and PDO. For SPI-6, a relatively stronger association exist and explains 23.8% and 28.2%, respectively of the variability in ENSO over northern Brazil (Figs. 10a-b). Other regions (ISPI-4, ISPI-7, Fig. 3) also show significant relationship (Figs. 10c-d). In SPE-12, the influence of ENSO is also notable (Fig. 10e-h) but relatively stronger in northern Brazil explaining 20% (R^2%) of observed variability in ENSO (Fig. 10g, cf. ISPI-4, Fig. 4). The MERRA indicator captures the influence of ENSO and PDO in the region (Figs. 11a-e). The influence of ENSO ($R^2 = 15.1\%$) and

PDO ($R^2 = 17.1\%$ and $R^2 = 18.1\%$) are more pronounced in the east and central regions of Brazil (Fig. 11a-b and d-e, cf. ISPI-1/ISPI-4, Fig. 5). This diagnostics confirm the interplay between interactions of ENSO and PDO with meteorological processes in Brazil and shows significant relationship (Figs. 11a-b). A simple linear regression of these indicators with climate modes show that generally, the SPI-6 can be used to extract and identify the influence of these teleconnections (PDO and ENSO) better than other indicators. The relationships of these indicators with teleconnections as reported here are fundamentally linear but these indications can interact in non-linear ways with climate modes.

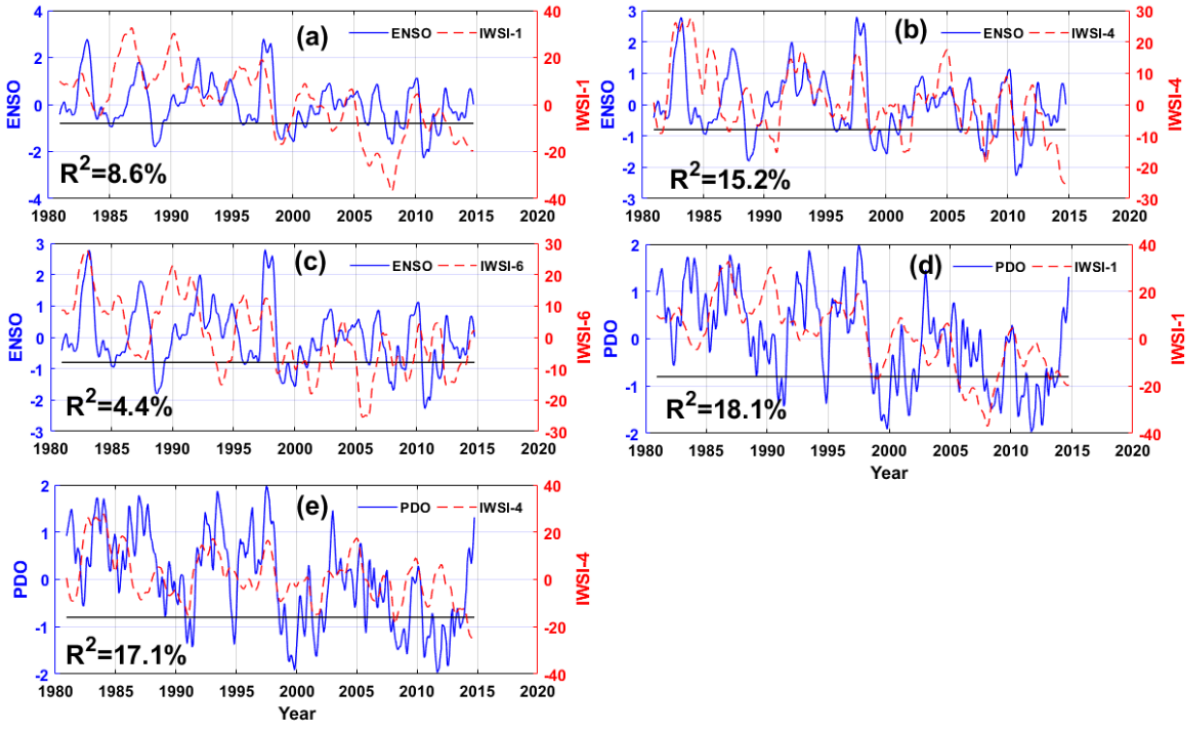

Figure 11: Influence of ENSO and PDO on evolutionary patterns of MERRA-derived drought indicator. Similar to Fig. 10 above the (a-e) relationship of ENSO with the MERRA indicator is based on linear regression.

For each of the hot spots identified in Section 3.1, the influence of global climate was further diagnosed by using a suite of climate modes as independent variables in the SVMR scheme to predict the temporal variations associated with the hot spot. The results of the observed and predicted drought indicators, which make a case for the coupled variability between climate teleconnection patterns and drought events in some regions of Brazil are summarised in Table 1. While there is an obvious evidence of the interplay between interactions of teleconnection patterns with the temporal evolutions of drought (Figs. 12a-f), the synthesis of all climate teleconnection indices as predictors of extreme events show that the Brazilian sub-region is a

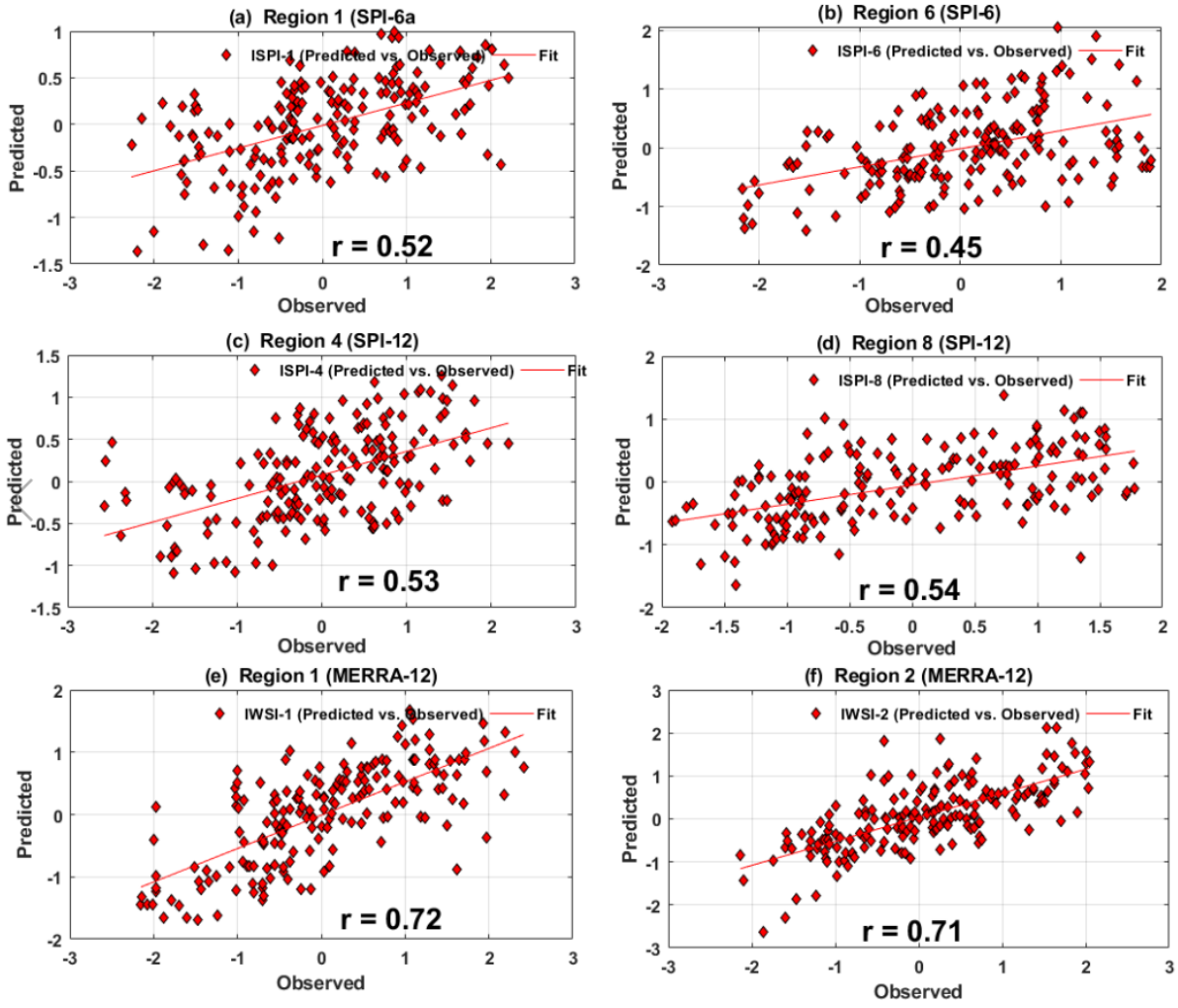

Figure 12: The influence of climate oscillations on the temporal patterns of regionalised modes of SPI-6 (a-b), SPI-12 (c-d) and MERRA SPI-12 (e-f) indicators using SVMR. Relationship between observed and predicted drought indicator uses all seven climate teleconnection indices as predictands in the SVMR scheme based on the hold-out cross validation partition.

complex web of climatic hot spot (Table 1). From the regression coefficients (SPI-6/SPI-12 vs all climate modes), ENSO, PDO, and AMO were the leading drivers of drought patterns in the region. However, the SVMR coefficients also revealed the influence of QBO AMM, MJO in the hot spots. As with SPI drought indices, the regression coefficients of MERRA indicator for example confirm the contributions of ENSO, MJO, AMO and AMM in Brazil. As illustrated in Figs. 12e-f, the MERRA indicator, with a considerable correlation ($r = 0.72$ and $r = 0.71$) between observed and predicted is a more suitable drought metric to understand the impacts of global climate on extreme events compared to other SPIs (Figs. 12a-d).

4. Discussion

4.1. Interactions of climate teleconnection patterns with hydrological hot spots

The statistical rotation of drought indicators has recently been employed in the analytical and quantitative assessment of the effectiveness of various drought indicators, particularly in exploring inconsistencies emanating from topographical variations, gauge density, and model forcing parameters on drought impacts (Agutu et al., 2020). Given the considerable variability in the distribution of rainfall and the role of global climate tele-connection patterns on extreme events at different scales (e.g., Cook et al., 2018, Kiem et al., 2016, Paeth et al., 2012), a spatio-temporal approach to drought analysis through localization and regionalization is thus crucial. It is with this in mind that cumulant rotation was employed to localize and characterize spatial and temporal variability of drought evolution over Brazil. To avoid generalizing drought intensities, severities, and its cascading impacts over largely heterogenous regions, this study has demonstrated the importance of this approach over Brazil where strong spatial variability of rainfall at annual scale along climatological gradients across region is obvious (cf. Fig. 1).

Localised SPI and MERRA patterns show that drought variability is relatively higher in the north and north-east Brazil. While each of the hydrological regions identified through the decomposition of drought indicators have unique response to climate teleconnections, the impact of time scales (i.e., SPI-6 and SPI-12) in extracting tele-connection influence also differ with region. For example, in the entire northern section of Brazil, SPI-6 extracts the influence of ENSO better than SPI-12 while the latter extracts tele-connection influence better than SPI-6 in the south of Brazil. Notably, as earlier mentioned, the SPI is widely recognised for its computational simplicity and ability to track meteorological (precipitation deficits), agricultural (soil moisture deficits leading to crop failure) and hydrological (abnormally low water levels, in lakes, reservoir levels, and groundwater) drought events based on different aggregation scales (e.g., Basu et al., 2017, Hayes et al., 2011, Mishra and Singh, 2010, McKee et al., 1995). As with other emerging drought indicators, the multi-scalar nature of SPI (e.g., SPI aggregated at 3 and 6 months can be used to characterize meteorological and agricultural droughts, respectively while 9 and 12 months aggregation can be used to capture hydrological droughts) allows the monitoring of impacts and understanding characteristics and propagation. On the one hand, this is crucial in the context of predicting drought early warning systems. On the other hand, it can aid the assessment of key drivers, be it anthropogenic or climatic, e.g., global climate teleconnection patterns. Depending on regions, SPI accumulation on different time scales (e.g., 3, 6, 9 and 12 months) could have different response or

association with climate teleconnection indices. This study confirms that for Brazil and is consistent with reports from other regions (e.g., Ndehedehe et al., 2016). Ultimately, the key message is the predominant influence of ENSO in the north/north-east and south of Brazil. However, in addition to these regions and the region that encompasses the central Brazil, the MERRA-based drought indicator reveals the significant contribution of PDO and ENSO. From a machine learning perspective that utilizes all climate modes to predict the temporal variations of drought indicators in all regions identified in Section 3, i.e, based on the hold-out method of cross validation, there is evidence to suggest global multi-scale climate influence on drought evolutions. These climatic influence range from multi-decadal (AMO and PDO) to quasi-biennial (QBO, inter-annual oscillations (ENSO) and other climate oscillation (AMM and MJO). In studying the influence of global climate on the temporal variations of extreme event over Brazil, the MERRA data is considerably promising and extracts the influence of these climate teleconnections better than the SPI (Table1).

It should be noted that identifying the role of these teleconnections in the region was enhanced by the combined use of machine learning and cumulant rotation to localize drought indicators. Third order statistics such as the PCA (Jolliffe, 2002) is now emerging in drought studies after it was first introduced by Karl and Koscielny (1982) to analysed long-term Palmer Drought Severity Indices over the United States. For example, based on PCA, the study by Santos et al. (2010) confirmed that drought events vary in time and space. They showed that the south of Portugal had more frequent cycles of dry events (every 3.6 years) compared to the northern region where severe to extreme droughts occurred approximately every 13.4 years. However, the robustness of fourth order statistical methods such as cumulant rotation in drought analysis is not well known and was explored here to localize drought signals, complementing existing frameworks of multivariate methods that have been deployed for routine analysis of drought variability. The innate potential of advanced statistical rotation was recently demonstrated in East Africa where it was used to assess groundwater changes in nine major aquifers (Agutu et al., 2019).

The influence of climate teleconnections on the hydrology of South America is well known (e.g., Ndehedehe and Ferreira, 2020b, Peng et al., 2019, Erfanian et al., 2017, Linage et al., 2013). In Brazil, ENSO and tropical North Atlantic sea surface temperature field play major roles in drought occurrence (Marengo et al., 2018). And consistent with our study Costa et al. (2016) acknowledged the influence of ENSO on rainfall variability and droughts in eastern north-east Brazil, specifically highlighting the roles of Pacific and Atlantic on extreme

events. Arguably, ENSO is the largest inter-annual climate phenomenon and its influence on hydro-meteorological processes and drought events has been widely studied and acknowledged globally (e.g., Costa et al., 2016, Paeth et al., 2012, Williams and Hanan, 2011, White et al., 2004, Nicholson et al., 2000). However, the observed coefficients in the SVMR scheme, show that apart from ENSO, AMO, PDO, and AMM explained significant variability in the predicted drought indicator, thus emphasizing the key role of the Atlantic and Pacific in the hydrological hot spots identified in Brazil. To further buttress the influence of these oceans, for example, the regression coefficients did not change significantly when only AMO, ENSO, and PDO were used as predictors in SVMR model, especially in the north/north-east regions. Given the linear relationship between these teleconnections and localized drought indicators, the continued application of this method in drought characterization is important to predict and track the ocean-atmosphere interactions and low frequency climate oscillations associated with drought episodes in Brazil.

4.2. Drought statistics and the role of science and policy solutions in risk mitigation

In the light of several precarious drought events, similar to other emerging economies, the Brazilian government has responded to several critical climatic thresholds through the construction of massive water infrastructures. As at 2016, for example, a total of 19,361 man-made reservoirs used for irrigation and hydropower, among others existed in Brazil (ANA, 2017). In our drought analysis, two periods exist when drought affected areas reached and exceeded 50%. Based on the MERRA indicator, the first was during the 1998/1999 period and the second occurred between 2012 and 2016. It was mentioned in Getirana (2016) that the former was the cause of the biggest energy crisis that occurred in Brazil while the impacts of the $2012 - 2015$ extreme droughts have been fully detailed and includes, major freshwater crises, groundwater depletion, agricultural losses, depletion of moisture influx from the Amazon basin, among several other causes (e.g., Ferreira et al., 2018, Marengo et al., 2018, Awange et al., 2016, Getirana, 2016). Drought statistics as provided here could be a key step towards improving water allocation systems thus diminishing the impacts of extreme droughts in the region. In this study, the spatio-temporal variability of drought indicators and mean drought duration over Brazil in the last 35 years can be useful parameters to strengthen policy efforts in water management and allocation. Our SPI analysis show high frequency in the temporal evolutions of drought in the north-east Brazil with prolonged events noted between 2008 and 2015 and coincides with periods of groundwater depletion in some aquifer systems in the north-

east region (Gonçalves et al., 2020, Melati et al., 2019). As key hot spots of climatic influence, the north-east region of Brazil has a long history of water-related environmental issues, which for the most part is linked to limited rainfall and climate-induced extreme prolonged drought.

The key solutions put forward during risk mitigation is effective management of water resources. This approach should encompass the wider challenges affecting drought monitoring and management. Thus, efficient drought management and monitoring of water resources and designing response policies and strategies at national, regional and international levels are required for building resilience to droughts (Haile et al., 2019, Sheffield et al., 2014). These activities could further help to minimize the natural climate variabilities and anthropogenic influences in aggravating drought conditions (Haile et al., 2019). Further, building a drought-resilient economy is needed for drought-vulnerable societies as it can help for better preparedness for coping, awareness for early warning of droughts (e.g., Sheffield et al., 2014). These could help to reduce the future impacts of droughts on socio-economic activities and the natural ecosystem functions across. Furthermore, mitigation strategies, risk-based decisions, and science-based adaptive approaches are also expected key outcomes aimed at increasing drought preparedness (e.g., Ndehedehe et al., 2019). These outcomes may play a role not only in raising the level of drought preparedness but could promote region-specific drought risk-management policy solutions. Some of these solutions may range from effective freshwater-based management decisions and drought mitigation strategies to important complementary interventions, such as insurance programs and government aids to affected regions and rural agro-communities to help cushion the effects of drought-inflicted calamity and losses. Through stake-holder participation, public policy and outcry, this is currently being implemented in some drought-prone regions of developed and emerging economies. For example, public policy framework on drought response in Brazil has been designed to allocate funds and water distribution to small scale farmers to help cushion drought impacts (Brito et al., 2018). Water transfer and additional water storage infrastructure are other management initiatives to build drought resilience.

5. Conclusions

Direct impacts of extreme droughts on contemporary human societies have resulted in the increased interest in region-specific assessments of droughts and the need to build drought resilience. In this study, a novel two-step regularization procedure that combines advanced multivariate methods with support vector machine regression was employed to assess and iden-

tify hydrological regions in Brazil where extreme events (droughts) are significantly associated with indices of oceanic variability. The results from this study are summarised as follows;

(i) Statistical rotation of drought indicators (SPI and MERRA) show that drought variability is relatively higher in the extreme north and north-east region of Brazil. The influence of strong spatial variability in rainfall at all temporal scales across regions modulate drought magnitudes and its properties. This largely explains the increased frequency and higher variability of drought events in the semi-arid north-east region compared to the humid (Amazon and environs) regions of Brazil. Areas along the Amazon and humid parts of Brazil show considerable and continued decline in MERRA indicator since 1980 and also highlights the major drought events (1998/1999, 2005, and $2012 - 2015$) that ravaged the region.

(ii) The predominance of extreme drought events from drought indicators agree that more than 50% of Brazil was affected by the 1998/1999 drought. But the extreme drought of 2015 was the worst since 1980 affecting approximately 70% of the country. The MERRA indicator shows this was an all-year (January-December) event with at least 60% areas being under drought every month.

(iii) SPI analysis show high frequency in the temporal evolutions of drought in the north-east Brazil with prolonged events noted between 2008 and 2015 and coincides with periods of groundwater depletion in some aquifer systems in the region. Mean drought duration appear to be prevalent and higher around the Amazon and north-west sections of Brazil but generally less frequent in some areas of the Amazon basin. On a longer time scale, this drought duration is higher in the central Amazon area and ranges from $8 - 10$ months compared to areas located on the south and north-east Brazil. But the spatial distribution of drought intensities over Brazil tend to be fairly similar except in some north-west regions.

(iv) In the climatic hotspots identified in Brazil (north/north-east and south of Brazil), ENSO, AMO, and PDO are the predominant climate teleconnections significantly associated with droughts. However, the significant contributions of MJO, AMM, and other multi-scale climate modes were detected in the SVMR scheme, thus emphasizing the role of the Atlantic and Pacific in these climatic hot spots. The impact of timescales (e.g. SPI-6 or SPI-12) in extracting tele-connection influence on droughts is noted but

overall the MERRA indicator is considerably promising and extracts climate influence better than the SPI.

(v) Some of the differences between SPI and MERRA indicators demonstrate the intrinsic hydrological response of surface hydrology and land surface conditions in some semi-arid/or moderately humid regions to extreme climate events such as drought. Due to a possible impacts of land surface processes, such as temperature and groundwater withdrawals for irrigation as is the case in Brazil, MERRA-drought indicator therefore will be more reliable to capture these impacts because of the inclusion of soil moisture and latent heat flux in the model. In this regard, precipitation-based drought indicator might be restricted because of complex hydrological processes (e.g., infiltration and flow dynamics) that could be linked to interactions between land surface-moisture fluxes and the atmosphere under an extreme drought scenario.

(vi) Identifying the role of climate teleconnections in Brazil was enhanced by the combined use of machine learning and cumulant rotation to localize drought indicators. Hence, the continued application of this method in drought characterization is important to improve knowledge on the ocean-atmosphere interactions and low frequency climate oscillations associated with drought episodes in several sub-regions of Brazil. We note that reanalysis data such as MERRA could be restricted in some regions because of the lack of sufficient direct observations for adequate initialization of its outputs. However, the novel two-step regularization framework developed in this study using the GPCC-derived SPI confirms the importance of the Pacific and Atlantic oceans on drought evolutions in Brazil.

Acknowledgments

The authors are grateful to NASA, and NOAA, for all the data used in this study. The comments of two anonymous reviewers were very useful and are greatly appreciated.

References

Agutu, N., Awange, J., Ndehedehe, C., Kirimi, F., and Kuhn, M. (2019). GRACE-derived groundwater changes over Greater Horn of Africa: temporal variability and the potential for irrigated agriculture. *Science of The Total Environment*, 693:133467. doi:10.1016/j.scitotenv.2019.07.273.

Agutu, N., Awange, J., Ndehedehe, C., and Mwaniki, M. (2020). Consistency of agricultural drought characterization over Upper Greater Horn of Africa (1982–2013):topographical, gauge density, and model forcing influence. *Science of The Total Environment*, 709:135149. doi:10.1016/j.scitotenv.2019.135149.

Agutu, N., Awange, J., Zerihun, A., Ndehedehe, C., Kuhn, M., and Fukuda, Y. (2017). Assessing multi-satellite remote sensing, reanalysis, and land surface models' products in characterizing agricultural drought in East Africa. *Remote Sensing of Environment*, 194(0):287–302. doi:10.1016/j.rse.2017.03.041.

Ali, A. and Lebel, T. (2009). The Sahelian standardized rainfall index revisited. *International Journal Of Climatology*, 29:1705–1714. doi:10.1002/joc.1832.

ANA (2017). Brazilian water resources report 2017. *National Water Agency, Brazil*.

Awange, J. L., Mpelasoka, F., and Goncalves, R. M. (2016). When every drop counts: Analysis of droughts in Brazil for the 1901-2013 period. *Science of The Total Environment*, 566-567:1472 – 1488. doi:10.1016/j.scitotenv.2016.06.031.

Basu, R., Singh, C. K., and Eslamian, S. (2017). Cause and occurrence of drought, in handbook of drought and water scarcity, vol. 1: Principles of drought and water scarcity. *Taylor and Francis, CRC Press, USA*, pages 137–148.

Bazrafshan, J., Hejabi, S., and Rahimi, J. (2014). Drought monitoring using the multivariate standardized precipitation index (MSPI). *Water Resources Mangagement*, 28:1045–1060. doi:10.1007/s11269-014-0533-2.

Benson, C. and Clay, E. (1994). The impact of drought on sub-sahara africa. *Overseas Development Institute*, 77. Retrieved from :https://www.odi.org/sites/odi.org.uk/files/odi-assets/publications-opinion-files/6988.pdf on 5th December, 2017.

741 Brito, S. S. B., Cunha, A. P. M. A., Cunningham, C. C., Alvalá, R. C., Marengo,
742 J. A., and Carvalho, M. A. (2018). Frequency, duration and severity of drought in the
743 semiarid Northeast Brazil region. *International Journal of Climatology*, 38(2):517–529.
744 doi:10.1002/joc.5225.

745 Brown, C. and Lall, U. (2006). Water and economic development: The role of variability and
746 a framework for resilience. *Natural Resources Forum*, 30(4):306–317.

747 Cardoso, J.-F. (1991). Super-symmetric decomposition of the fourth-order cumulant ten-
748 sor, blind identification of more sources than sensors. Retrieved from:http://perso.telecom-
749 paristech.fr/ cardoso/Papers.PDF/icassp91.pdf. Accessed 15 January 2016.

750 Cardoso, J. F. (1999). High-Order contrasts for Independent Component Analysis. *Neural*
751 *Computation*, 11:157–192.

752 Cardoso, J. F. and Souloumiac, A. (1993). Blind beamforming for non-gaussian signals. *IEE*
753 *Proceedings*, 140(6):362–370.

754 Chen, T., de Jeu, R., Liu, Y., van der Werf, G., and Dolman, A. (2014). Using satellite based
755 soil moisture to quantify the water driven variability in NDVI: A case study over mainland
756 Australia. *Remote Sensing of Environment*, 140:330 – 338. doi:10.1016/j.rse.2013.08.022.

757 Common, P. (1994). Independent component analysis, A new concept? *Signal Processing*,
758 36:287–314.

759 Cook, B. I., Mankin, J. S., and Anchukaitis, K. J. (2018). Climate change and drought: From
760 past to future. *Current Climate Change Reports*, 4(2):164–179. doi:10.1007/s40641-018-
761 0093-2.

762 Cortes, C. and Vapnik, V. (1995). Support vector networks. *Machine Learning*, 20:273–297.

763 Costa, D. D., da Silva Pereira, T. A., Fragoso, C. R., Madani, K., and Uvo, C. B. (2016).
764 Understanding drought dynamics during dry season in Eastern Northeast Brazil. *Frontiers*
765 *in Earth Science*, 4:69. doi:10.3389/feart.2016.00069.

766 de Linage, C., Famiglietti, J. S., and Randerson, J. T. (2014). Statistical prediction of terres-
767 trial water storage changes in the Amazon Basin using tropical Pacific and North Atlantic
768 sea surface temperature anomalies. *Hydrology and Earth System Sciences*, 18(6):2089–2102.
769 doi:10.5194/hess-18-2089-2014.

770 Diaz, V., Corzo, G., Lanen, H. A. V., and Solomatine, D. P. (2019). Spatiotemporal drought
771 analysis at country scale through the application of the STAND Toolbox. pages 77 – 93.
772 doi:10.1016/B978-0-12-811689-0.00004-5.

773 Erfanian, A., Wang, G., and Fomenko, L. (2017). Unprecedented drought over tropical south
774 america in 2016: significantly under-predicted by tropical sst. *Scientific Reports*, 7(5811).
775 doi:10.1038/s41598-017-05373-2.

776 Farahmand, A. and AghaKouchak, A. (2015). A generalized framework for deriving non-
777 parametric standardized drought indicators. *Advances in Water Resources*, (76):140–145.
778 doi:/10.1016/j.advwatres.2014.11.012.

779 Ferreira, V., Montecino, H., Ndehedehe, C., Heck, B., Gong, Z., Westerhaus, M., and de Fre-
780 itas, S. (2018). Space-based observations of crustal deflections for drought characterization in
781 brazil. *Science of The Total Environment*, 644:256–273. doi:10.1016/j.scitotenv.2018.06.277.

782 Frappart, F., Papa, F., Guntner, A., Werth, S., da Silva, J. S., Tomasella, J., Seyler, F.,
783 Prigent, C., Rossow, W. B., Calmant, S., and Bonnet, M.-P. (2011). Satellite-based estimates
784 of groundwater storage variations in large drainage basins with extensive floodplains. *Remote*
785 *Sensing of Environment*, 115(6):1588–1594. doi:10.1016/j.rse.2011.02.003.

786 Getirana, A. (2016). Extreme water deficit in brazil detected from space. *Journal of Hydrom-*
787 *eteorology*, 17(2):591–599. doi:10.1175/JHM-D-15-0096.1.

788 Gonçalves, R. D., Stollberg, R., Weiss, H., and Chang, H. K. (2020). Using GRACE to
789 quantify the depletion of terrestrial water storage in Northeastern Brazil: The Urucuia
790 Aquifer System. *Science of The Total Environment*, 705:135845.

791 Haile, G. G., Tang, Q., Leng, G., Jia, G., Wang, J., Cai, D., Sun, S., Baniya, B., and Zhang,
792 Q. (2020). Long-term spatiotemporal variation of drought patterns over the Greater Horn of
793 Africa. *Science of The Total Environment*, 704:135299. doi:10.1016/j.scitotenv.2019.135299.

794 Haile, G. G., Tang, Q., Sun, S., Huang, Z., Zhang, X., and Liu, X. (2019). Droughts
795 in East Africa: causes, impacts and resilience. *Earth-Science Reviews*, 193:146 – 161.
796 doi:10.1016/j.earscirev.2019.04.015.

797 Haley, M. R. (2017). K-fold cross validation performance comparisons of six naive portfo-
798 lio selection rules: how naive can you be and still have successful out-of-sample portfolio
799 performance? *Annals of Finance*, 13(3):341–353. doi:10.1007/s10436-017-0301-4.

Hall, J. W., Grey, D., Garrick, D., Fung, F., Brown, C., Dadson, S. J., and Sadoff, C. W. (2014). Coping with the curse of freshwater variability. *Science*, 346(6208):429–430. doi:10.1126/science.1257890.

Hao, Z. and AghaKouchak, A. (2014). A nonparametric multivariate multi-index drought monitoring framework. *Journal of Hydrometeorology*, 15(1):89–101. doi:10.1175/JHM-D-12-0160.1.

Hayes, M., Svoboda, M., Wall, N., and Widhalm, M. (2011). The Lincoln Declaration On Drought Indices: Universal Meteorological Drought Index Recommended. *Drought Mitigation Center Faculty Publications*. Accessed from http://digitalcommons.unl.edu/droughtfacpub/14 on 9th June 2020.

Jolliffe, I. T. (2002). Principal component analysis (second edition). *Springer Series in Statistics*. Springer, New York.

Jung, H. C., Getirana, A., Policelli, F., McNally, A., Arsenault, K. R., Kumar, S., Tadesse, T., and Peters-Lidard, C. D. (2017). Upper Blue Nile basin water budget from a multi-model perspective. *Journal of Hydrology*, 555:535 – 546. doi:10.1016/j.jhydrol.2017.10.040.

Karl, T. R. and Koscielny, A. J. (1982). Drought in the United States: 1895–1981. *Journal of Climatology*, 2(4):313–329. doi:10.1002/joc.3370020402.

Kiem, A. S., Johnson, F., Westra, S., van Dijk, A., Evans, J. P., O'Donnell, A., Rouillard, A., Barr, C., Tyler, J., Thyer, M., Jakob, D., Woldemeskel, F., Sivakumar, B., and Mehrotra, R. (2016). Natural hazards in Australia: droughts. *Climatic Change*, 139(1):37–54. doi:10.1007/s10584-016-1798-7.

Kurnik, B., Kajfež-Bogataj, L., and Horion, S. (2015). An assessment of actual evapotranspiration and soil water deficit in agricultural regions in Europe. *International Journal of Climatology*, 35(9):2451–2471. doi:10.1002/joc.4154.

Linage, C., Kim, H., Famiglietti, J. S., and Yu, J.-Y. (2013). Impact of pacific and atlantic sea surface temperatures on interannual and decadal variations of GRACE land water storage in tropical South America. *Journal of Geophysical Research: Atmospheres*, 118(19):10,811–10,829. doi:10.1002/jgrd.50820.

828 Mao, Y., Wu, Z., He, H., Lu, G., Xu, H., and Lin, Q. (2017). Spatio-temporal analysis of
829 drought in a typical plain region based on the soil moisture anomaly percentage index.
830 *Science of The Total Environment*, 576:752 – 765. doi:10.1016/j.scitotenv.2016.10.116.

831 Marengo, J. A., Alves, L. M., Alvala, R. C., Cunha, A. P., Brito, S., and Moraes, O. L.
832 (2018). Climatic characteristics of the 2010-2016 drought in the semiarid Northeast Brazil
833 region. *Anais da Academia Brasileira de Ciencias*, 90:1973 – 1985. doi:10.1590/0001-
834 3765201720170206.

835 Marengo, J. A., Torres, R. R., and Alves, L. M. (2017). Drought in Northeast Brazil—
836 past, present, and future. *Theoretical and Applied Climatology*, 129(3):1189–1200.
837 doi:10.1007/s00704-016-1840-8.

838 Martinez, W. L. and Martinez, A. R. (2005). *Exploratory Data Analysis with MATLAB*.
839 Computer Science and Data Analysis Series. Chapman and Hall/CRC Press LLC, UK.

840 McKee, T. B., Doeskin, N. J., and Kieist, J. (1993). The relationship of
841 drought frequency and duration to time scales. *Conference on Applied Climatol-*
842 *ogy, American Meteorological Society,Boston, Massachusetts*, pages 179–184. Retrieved
843 from:www.ccc.atmos.colostate.edu/relationshipofdroughtfrequency.pdf. Accessed 27 June,
844 2014.

845 McKee, T. B., Doeskin, N. J., and Kieist, J. (1995). Drought monitoring with multiple
846 time scales. *Conference on Applied Climatology, American Meteorological Society, Boston,*
847 *Massachusetts*, pages 233–236. Retrieved from:www.southwestclimatechange.org/node/911.
848 Accessed 13 July, 2014.

849 Melati, M. D., Fleischmann, A. S., Fan, F. M., Paiva, R. C. D., and Athayde, G. B. (2019).
850 Estimates of groundwater depletion under extreme drought in the Brazilian semi-arid region
851 using GRACE satellite data: application for a small-scale aquifer. *Hydrogeology Journal*,
852 27(8):2789–2802. doi:10.1007/s10040-019-02065-1.

853 Mishra, A. K. and Singh, V. P. (2010). A review of drought concepts. *Journal of Hydrology*,
854 391:202–216. doi:10.1016/j.jhydrol.2010.07.012.

855 Montazerolghaem, M., Vervoort, W., Minasny, B., and McBratney, A. (2016). Long-term
856 variability of the leading seasonal modes of rainfall in south-eastern Australia. *Weather and*
857 *Climate Extremes*, 13:1 – 14. doi:10.1016/j.wace.2016.04.001.

Ndehedehe, C. E., Agutu, N., Ferreira, V. G., and Getirana, A. (2020). Evolutionary drought patterns over the Sahel and their teleconnections with low frequency climate oscillations. *Atmospheric Research*, 233:104700. doi:10.1016/j.atmosres.2019.104700.

Ndehedehe, C. E., Agutu, N. O., Okwuashi, O. H., and Ferreira, V. G. (2016). Spatio-temporal variability of droughts and terrestrial water storage over Lake Chad Basin using independent component analysis. *Journal of Hydrology*, 540:106–128. doi:10.1016/j.jhydrol.2016.05.068.

Ndehedehe, C. E., Anyah, R. O., Alsdorf, D., Agutu, N. O., and Ferreira, V. G. (2019). Modelling the impacts of global multi-scale climatic drivers on hydro-climatic extremes (1901–2014) over the Congo basin. *Science of The Total Environment*, 651:1569 – 1587. doi:10.1016/j.scitotenv.2018.09.203.

Ndehedehe, C. E., Awange, J., Kuhn, M., Agutu, N., and Fukuda, Y. (2017). Climate teleconnections influence on West Africa's terrestrial water storage. *Hydrological Processes*, 31(18):3206–3224. doi: 10.1002/hyp.11237.

Ndehedehe, C. E. and Ferreira, V. G. (2020a). Assessing land water storage dynamics over Southern America. *Journal of Hydrology*, 580:124339. doi:10.1016/j.jhydrol.2019.124339.

Ndehedehe, C. E. and Ferreira, V. G. (2020b). Identifying the footprints of global climate modes in time-variable gravity hydrological signals. *Climatic Change*, 159:481–502. 10.1007/s10584-019-02588-2.

Nicholson, S. E., Some, B., and Kone, B. (2000). An analysis of recent rainfall conditions in West Africa, including the rainy seasons of the 1997 El Niño and the 1998 La Niña years. *Journal of Climate*, 13(14):2628–2640. doi:10.1175/1520-0442(2000)013<2628:AAORRC>2.0.CO;2.

Okwuashi, O. and Ndehedehe, C. (2017). Tide modelling using support vector machine regression. *Journal of Spatial Science*, 62(1):29–46. doi:10.1080/14498596.2016.1215272.

Paeth, H., Fink, A., Pohle, S., Keis, F., Machel, H., and Samimi, C. (2012). Meteorological characteristics and potential causes of the 2007 flood in sub-Saharan Africa. *International Journal of Climatology*, 31:1908–1926. doi:10.1002/Joc.2199.

Peng, Q., Xie, S., and Wang, D. e. a. (2019). Coupled ocean-atmosphere dynamics of the 2017 extreme coastal El Niño. *Nature Communications*, 10(298). https://doi.org/10.1038/s41467-018-08258-8.

Reichle, R. H., Koster, R. D., Lannoy, G. J. M. D., Forman, B. A., Liu, Q., Mahanama, S. P. P., and TourÃ©, A. (2011). Assessment and enhancement of MERRA land surface hydrology estimates. *Journal of Climate*, 24(24):6322–6338. doi:10.1175/JCLI-D-10-05033.1.

Rienecker, M. M., Suarez, M. J., Gelaro, R., Todling, R., Bacmeister, J., Liu, E., Bosilovich, M. G., Schubert, S. D., Takacs, L., Kim, G.-K., Bloom, S., Chen, J., Collins, D., Conaty, A., da Silva, A., Gu, W., Joiner, J., Koster, R. D., Lucchesi, R., Molod, A., Owens, T., Pawson, S., Pegion, P., Redder, C. R., Reichle, R., Robertson, F. R., Ruddick, A. G., Sienkiewicz, M., and Woollen, J. (2011). MERRA: NASA's modern-era retrospective analysis for research and applications. *Journal of Climate*, 24(14):3624–3648. doi:10.1175/JCLI-D-11-00015.1.

Rippey, B. R. (2015). The U.S. drought of 2012. *Weather and Climate Extremes*, 10(Part A):57 – 64. doi:10.1016/j.wace.2015.10.004.

Santos, J. a. F., Pulido-Calvo, I., and Portela, M. M. (2010). Spatial and temporal variability of droughts in Portugal. *Water Resources Research*, 46(3):W03503. doi:10.1029/2009WR008071.

Schneider, U., Becker, A., Finger, P., Meyer-Christoffer, A., Ziese, M., and Rudolf, B. (2014). GPCC's new land surface precipitation climatology based on quality-controlled in situ data and its role in quantifying the global water cycle. *Theoretical and Applied Climatology*, 115(1-2):15–40. doi:10.1007/s00704-013-0860-x.

Sheffield, J., Wood, E. F., Chaney, N., Guan, K., Sadri, S., Yuan, X., Olang, L., Amani, A., Ali, A., Demuth, S., and Ogallo, L. (2014). A drought monitoring and forecasting system for Sub-Sahara African water resources and food security. *Bulletin of the American Meteorological Society*, 95(6):861–882. doi:10.1175/BAMS-D-12-00124.1.

Smola, A. J. and Schölkopf, B. (2004). A tutorial on support vector regression. *Statistics and Computing*, 14(3):199–222. doi:10.1023/B:STCO.0000035301.49549.88.

Snedecor, G. W. and Cochran, W. G. (1989). Statistical methods. *Iowa State University Press*, 8th Edition.

Spinoni, J., Naumann, G., Carrao, H., Barbosa, P., and Vogt, J. (2014). World drought frequency, duration, and severity for 1951–2010. *International Journal of Climatology*, 34(8):2792–2804. doi:10.1002/joc.3875.

Sullivan, C. A. (2011). Quantifying water vulnerability: a multi-dimensional approach. *Stochastic Environmental Research and Risk Assessment*, 25(4):627–640. doi:10.1007/s00477-010-0426-8.

Sun, T., Ferreira, V. G., He, X., and Andam-Akorful, S. A. (2016). Water availability of São Francisco river basin based on a space-borne geodetic sensor. *Water*, 8(5).

Theis, F. J., Gruber, P., Keck, I. R., Meyer-bäse, A., and Lang, E. W. (2005). Spatiotemporal blind source separation using double-sided approximate joint diagonalization. In *In Proc. EUSIPCO 2005*.

van der Molen, M., Dolman, A., Ciais, P., Eglin, T., Gobron, N., Law, B., Meir, P., Peters, W., Phillips, O., Reichstein, M., Chen, T., Dekker, S., Doubková, M., Friedl, M., Jung, M., van den Hurk, B., de Jeu, R., Kruijt, B., Ohta, T., Rebel, K., Plummer, S., Seneviratne, S., Sitch, S., Teuling, A., van der Werf, G., and Wang, G. (2011). Drought and ecosystem carbon cycling. *Agricultural and Forest Meteorology*, 151(7):765 – 773. doi:10.1016/j.agrformet.2011.01.018.

Vapnik, V. (1995). The nature of statistical learning theory. *Springer*. New York, NY:.

Wang, F., Wang, Z., Yang, H., and Zhao, Y. (2018). Study of the temporal and spatial patterns of drought in the Yellow River basin based on SPEI. *Science China Earth Sciences*, 61(8):1098–1111. doi:10.1007/s11430-017-9198-2.

Wauters, M. and Vanhoucke, M. (2014). Support vector machine regression for project control forecasting. *Automation in Construction*, 47:92 – 106. doi:10.1016/j.autcon.2014.07.014.

White, W. B., Gershunov, A., Annis, J. L., McKeon, G., and Syktus, J. (2004). Forecasting Australian drought using Southern Hemisphere modes of sea-surface temperature variability. *International Journal of Climatology*, 24(15):1911–1927. doi:10.1002/joc.1091.

Wilks, D. (2011). Statistical methods in the atmospheric sciences. *Academic press*, (3rd Edition). USA.

Williams, C. A. and Hanan, N. P. (2011). ENSO and IOD teleconnections for African ecosystems: evidence of destructive interference between climate oscillations. *Biogeosciences*, 8(1):27–40.

945 Xu, L., Chen, N., and Zhang, X. (2019). Global drought trends under 1.5 and 2 °c warming.
946 *International Journal of Climatology*, 39(4):2375–2385. doi:10.1002/joc.5958.

947 Yang, J. and Cheng, Q. (2015). A comparative study of independent component analysis
948 with principal component analysis in geological objects identification. part ii: A case study
949 of Pinghe District, Fujian, China. *Journal of Geochemical Exploration*, 149:136 – 146.
950 doi:10.1016/j.gexplo.2014.11.014.

951 Yu, M., Li, Q., Hayes, M. J., Svoboda, M. D., and Heim, R. R. (2014). Are droughts be-
952 coming more frequent or severe in China based on the Standardized Precipitation Evap-
953 otranspiration Index: 1951–2010? *International Journal of Climatology*, 34(3):545–558.
954 doi:10.1002/joc.3701.

955 Zhang, Q., Qi, T., Singh, V. P., Chen, Y. D., and Xiao, M. (2015). Regional frequency
956 analysis of droughts in china: A multivariate perspective. *Water Resources Management*,
957 29(6):1767–1787. doi:10.1007/s11269-014-0910-x.

958 Ziehe, A. (2005). Blind source separation based on joint diagonalization of matrices
959 with applications in biomedical signal processing. *PhD thesis,Universitat Potsdam*.
960 Retrieved from:http://en.youscribe.com/catalogue/reports-and-theses/knowledge/blind-
961 source-separation-based-on-joint-diagonalization-of-matrices-1424347. Accessed 15 May
962 2015.